Arabian Journal of Chemistry 16 (2023) 105263

Contents lists available at ScienceDirect

Arabian Journal of Chemistry

journal homepage: www.sciencedirect.com

Review article

Anthraquinone-based porous organic polymers: From synthesis to applications in electrochemical energy conversion and storage

Ning Qi [a], Bin Yao [a,*], Hongfei Sun [a], Yuan Gao [a], Xingyan Liu [a], Fei Li [b,*]

[a] Chongqing Key Laboratory of Catalysis and New Environmental Materials, College of Environment and Resources, Chongqing Technology and Business University, Chongqing 400067, China
[b] State Key Laboratory of Fine Chemicals, Dalian University of Technology, Dalian 116024, China

ARTICLE INFO

Article history:
Received 3 March 2023
Accepted 10 September 2023
Available online 14 September 2023

Keywords:
Anthraquinone
Porous Organic Polymers
Energy Conversion and Storage
Electrocatalysis
Metal-ion Battery
Supercapacitors

ABSTRACT

Anthraquinone derivatives, owing to their widespread resources, high structural diversity and excellent electrochemical characteristics, are a class of useful carbonyl materials that actively participate in multiple electrochemical processes. Nonetheless, good solubility of small molecules in organic electrolyte solutions causes a gradual decline in the cycle stability of related devices. Incorporating anthraquinone subunit into porous organic polymers (POPs) not only resolve the solubility problem but also endow the corresponding polymers with larger specific surface areas and more stable rigid structures, which is significantly meaningful to enhance the accessibility of active sites and improve the cycle stability of electrochemical devices. Recently, electrochemical energy conversion and storage have attracted growing attention in both scientific research and practical applications, and anthraquinone-based POPs play vital roles in these processes. Therefore, this article systematically summarizes the recent advances of anthraquinone-based POPs in electrochemical energy conversion and storage. Firstly, the synthesis of anthraquinone-based POPs is discussed, which will provide detailed information on how to select monomers as well as reactions and how to optimize reaction conditions to gain the desired POPs. Secondly, the practical applications of anthraquinone-based POPs in electrochemical energy conversion and storage are evaluated in detail, in which the morphology manipulation and conductivity improvement will be emphatically elaborated. Finally, the future development trend is also briefly prospected.

Abbreviations: AAn, 1,5-Diaminoanthraquinone; AQDB, Anthraquinonediboronic acid bis(pinacol) ester; BC, 3,6-Dibromo-9-(4-bromophenyl)carbazole; BTA, Benzene-1,3,5-tricarbaldehyde; CMPs, Conjugated Microporous Polymers; COFs, Covalent Organic Frameworks; CO_2RR, CO_2 Electroreduction Reaction; CTF, Covalent Triazine Framework; DAAQ, 2,6-Diaminoanthraquinone; DBrAQ, 2,6-Dibromoanthraquinone; DEAQ, 2,6-Diethynylanthraquinone; DFAQ, 2,6-Diformylanthraquinone; DFT, Density Functional Theory; DHAQ, 2,6-Dihydroxyanthraquinone; EDLC, Electrical Double-Layer Capacitance; HATN-AP, 2,3,8,9,14,15-Hexacarboxyl hexaazatrinaphthalene trianhydrides; HBB, Hexakis(bromomethyl)benzene; HCCP, Hexachlorocyclotriphosphazene; HHTP, 2,3,6,7,10,11-Hexahydroxytriphenylene; LIBs, Lithium-ion batteries; OH-AAn, 1,5-Diamino-4,8-dihydroxyanthraquinone; OHP, Hydroxyl-ended Hyperbranched Polymer; PIBs, Potassium-ion batteries; POPs, Porous Organic Polymers; PTB, Phenyltriboronic acid tris(pinacol) ester; Py-T, 1,3,6,8-Tetraethynylpyrene; RHE, Reversible Hydrogen Electrode; S_{BET}, Brunauer–Emmett–Teller Surface Area; SEI, Solid Electrolyte Interphase; SF, 2,2′,7,7′-Tetrabromo-9,9′-spirobifluorene; SIBs, Sodium-Ion Batteries; S_NAr, Nucleophilic Aromatic Substitution Reaction; TA, Tris(4-bromophenyl)amine; TB, Tris(4-bromophenyl)benzene; TBrB, 1,2,4,5-Tetrabromobenzene; TBrDB, Tris(bromoduryl)borane; TBrPy, 1,3,6,8-Tetrabromopyrene; TCT, 2,4,6-Trichloro-1,3,5-triazine; TEB, 1,3,5-Triethynylbenzene; TFAQ, 2,3,6,7-tetrafluoroanthraquinone; TFBQ, Tetrafluoro-1,4-benzoquinone; TFP, 1,3,5-Triformylphloroglucinol; THB, 1,3,5-Trihydroxybenzene; TM, Tetrakis(4-bromophenyl)methane; TMB, 1,3,5-Trimethylbenzene; TPE-T, Tetrakis(4-ethynylphenyl)ethylene; TTF-fo, Tetraformyl-tetrathiafulvalene; TpOMe, 2,4,6-trimethoxy-1,3,5-benzenetricarbaldehyde.

* Corresponding authors.
E-mail addresses: yaobin@ctbu.edu.cn (B. Yao), lifei@dlut.edu.cn (F. Li).

Peer review under responsibility of King Saud University.

Production and hosting by Elsevier

https://doi.org/10.1016/j.arabjc.2023.105263
1878-5352/

1. Introduction

Organic quinone materials, owing to their high structure diversity and flexibility, tunable redox activity, good electrochemical reversibility and reaction rates, fast kinetics and high theoretical specific capacity (low M_w assisted with a $2e^-$ redox processes per quinone subunit), have emerged as important candidate materials for electrochemical energy conversion and storage (Häupler et al., 2015; Son et al., 2016; Han et al., 2019; Peng et al., 2019; Zhu et al., 2019; Symons 2021). Among various quinone derivatives (including benzoquinone, pentacenediquinone, pyrene-4,5,9,10-tetraone, anthraquinone, etc.), anthraquinone derivatives stand out since they have the advantages of much proper molecular size, easier to derivate, and better solubility for further processing. For instance, various anthraquinone-based small molecules have been tried in various battery devices (Zhao et al., 2016; Deng et al., 2020; Ruan et al., 2021; Fontmorin et al., 2022). However, good solubility of organic small molecules in electrolytes generally results in rapid performance decay upon long-term cycles. Multiple methods have been attempted to circumvent the solubility problem, including introducing polar groups, adding additives, grafting small molecules onto conductive carbons via either covalent or non-covalent methods, and polymerization methodology (Kim 2017; Zhao et al., 2017; Yang et al., 2021; Lu et al., 2022). Compared with the former three methods, the polymerization strategy has proven to be a much more efficient approach (Tang et al., 2018; Zhang et al., 2022). Hence, serving as building block, anthraquinone has been incorporated into various main-chain (Song et al., 2015; Pan et al., 2016; Li et al., 2019) and side-chain (Choi et al., 2011; Oka et al., 2021; Wang et al., 2021) polymers, and the resultant polymers play active roles in electrochemical energy storage.

The linear redox-active polymers have demonstrated their enhanced performances compared to those of small molecules. However, the performance fading is still inevitable over long-time operation owing to linear polymerization can only relieve rather than completely prevent the dissolution. Moreover, the common low specific surface area of linear polymers would cause sluggish kinetics, resulting in poor rate capability in batteries. In the past two decades, the rapid developments of porous organic polymers (POPs) (Das et al., 2017; Zhu et al., 2020), including hyper cross-linked polymers (HCPs)(Xu et al., 2013), fused aromatic networks (FANs) (Mahmood et al., 2019), conjugated microporous polymers (CMPs) (Lee and Cooper 2020; Luo et al., 2021) and covalent organic frameworks (COFs) (Geng et al., 2020; Geng et al., 2020), have been witnessed. They possess with the merits of high specific surface area, low mass density, easy functionalization, and high stability. Especially for their two-dimensional skeletons, they could not only prevent the polymers from dissolving but also provide suitable channels for mass transfer as well as abundant space as active sites. Consequently, they are promising material platforms for diverse applications including adsorption and separation, sensing, catalysis, environmental remediation, and energy conversion and storage (Evans et al., 2022). Anthraquinone derivatives have demonstrated their high structural diversity (e.g., abundant and tunable functional groups), superior electrochemical performances (such as enhanced electrochemical stability, high active-material utilization and facilitated redox kinetics). POPs are provided with good chemical stability and high specific surface areas. Incorporating anthraquinone subunit into POPs would render the resulting anthraquinone-based POPs excellent candidates to serve as important components in various electrochemical energy conversion and storage devices.

Actually, we realize that several literatures have described carbonyl polymers for energy storage applications (Tang et al., 2018; Amin et al., 2019; Cui et al., 2020; Wang et al., 2020; Zhang et al., 2021; Zhang et al., 2022). However, they're all comprehensive reviews that both linear and POPs are included. Moreover, these reviews generally cover many structural units such as benzoquinone, anthraquinone, pyrene-4,5,9,10-tetraone, and aromatic imides. From these limited reviews, we find it is difficult to gain a thorough understanding of the overall developments of anthraquinone-based POPs. Recently, reports on the synthesis of anthraquinone-based POPs and their applications in electrochemical energy conversion and storage are massively emerging. Considering the rapid developing trends of electrochemical energy conversion and storage and the great contributions of anthraquinone-based POPs, it is quite necessary to have a special review to summarize the overall developments on anthraquinone-based POPs. Herein, this article systematically highlights the recent advances in the synthesis of anthraquinone-based POPs and their particular applications in electrochemical energy conversion and storage.

2. Design and synthesis of anthraquinone-based POPs

As mentioned previously, proper conjugated molecular structure makes anthraquinone easily derivable. Taking the commercially available 2,6-diaminoanthraquinone (DAAQ) as a good example, it could be effectively transformed to 2,6-dibromoanthraquinone (DBrAQ), 2,6-diethynylanthraquinone (DEAQ), and anthraquinonediboronic acid bis(pinacol) ester (AQDB). Together with other monomers, they are all critical building blocks to occur various reactions to construct POPs bearing different functional groups and topologies. Especially for conjugated microporous polymers (CMPs) and covalent organic frameworks (COFs) which can be used in many fields, these monomers have demonstrated their great potentials. For the resultant POPs, a variety of analytical methods could be applied to confirm the desired structures, such as Fourier transform infrared (FT-IR) spectroscopy, solid-state ^{13}C nuclear magnetic resonance (^{13}C NMR) spectroscopy, scanning electron microscopy (SEM), high-resolution transmission electron microscopy (HRTEM), solid-state electronic absorption spectroscopy, and powder X-ray diffraction (PXRD) (Evans et al., 2022). For COF materials, PXRD together with theoretical simulations are combined to determine to layer packing modes (Geng et al., 2020). The Brunauer–Emmett–Teller surface area (S_{BET}) and pore size distributions of POPs are gained through N_2 sorption isotherm profiles. The chemical structure and porous structure characterizations of POPs will not be discussed in the following text unless absolutely necessary. According to different reaction types, this section will detailedly discuss how to reasonably select monomers bearing different functional groups as well as topological structures and how to optimize the reaction conditions to gain the desired anthraquinone-containing POPs.

2.1. Condensation reactions

Schiff-base chemistry has demonstrated its great potential in constructing COFs (Segura et al., 2016). In 2013, DeBlase (DeBlase et al., 2013) reported the preparation of the famous DAAQ-TFP COF via the reaction of DAAQ and 1,3,5-triformylphloroglucinol (TFP) using solvothermal synthesis method (Fig. 1A, the detailed synthesis information is listed in Table 1). Owing to the unique structure of TFP monomer, the resulting COF quickly transforms from an unstable enol-imine form to a more stable $\beta-$ ketoenamine form. Except for bearing the highest S_{BET} among imine- or enamine-based COFs at that time, DAAQ-TFP was also the firstly reported redox COF on account of the reversible electrochemical behavior of anthraquinone units. Although with more

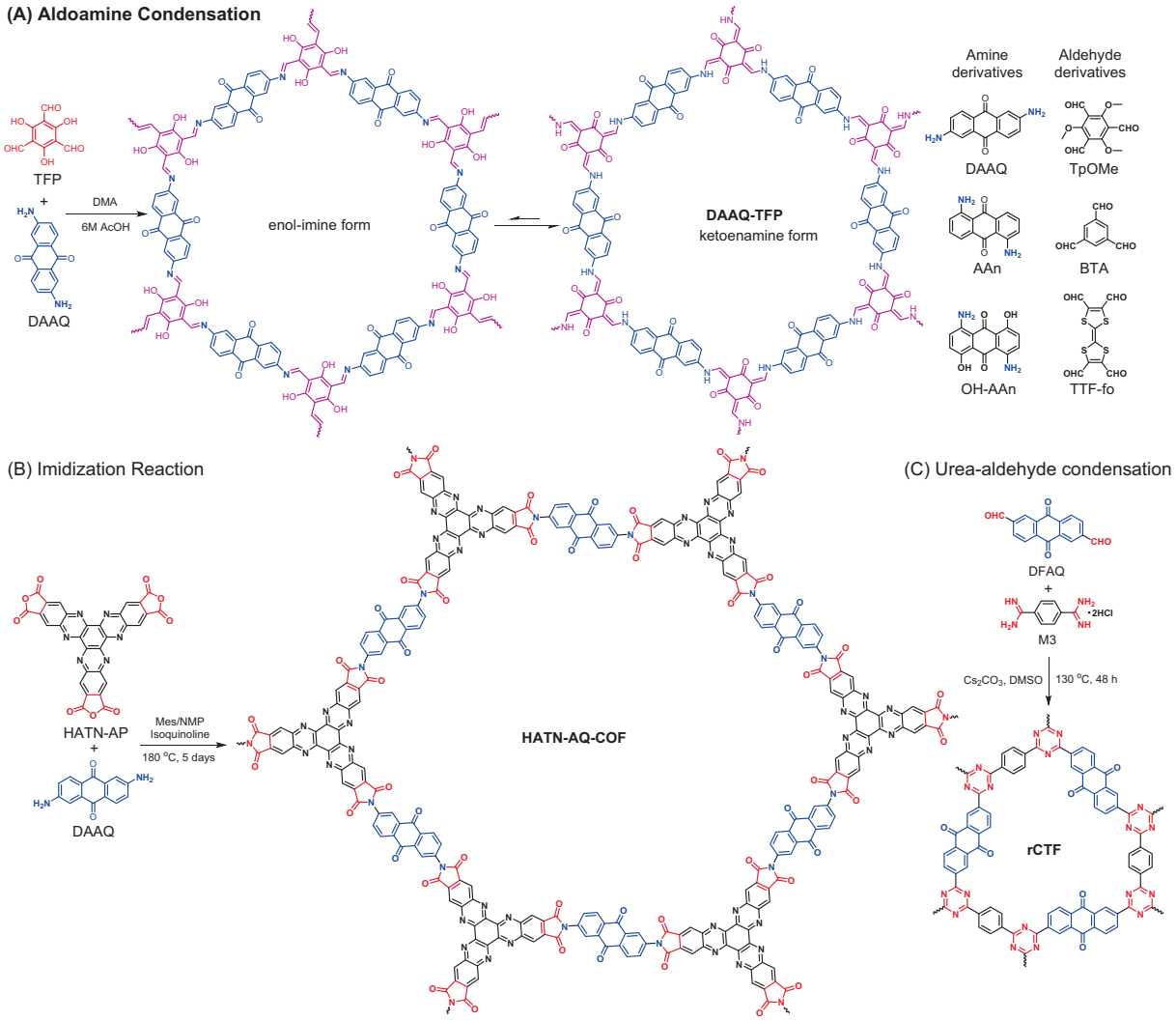

Fig. 1. Synthesis of of anthraquinone-based porous organic polymers via condensation reaction: (**A**) aldoamine condensation, (**B**) imidization reaction, and (**C**) urea-aldehyde condensation.

stable skeleton structure, the non-conjugative feature of β-ketoenamine in DAAQ-TFP might lead to sluggish electrochemical response compared with COFs with conjugated imine (C═N) bonds. Halder (Halder et al., 2018) and Zhao (Zhao et al., 2021) separately adopted 2,4,6-trimethoxy-1,3,5-benzenetricarbaldehyde (TpOMe) and benzene-1,3,5-tricarbaldehyde (BTA) as monomers to alleviate the problem. In addition to improving the planar characteristics of COF skeletons, taking donor–acceptor alternate connection mode is another alternative approach to enhance electrochemical kinetics. Li et al. (Li et al., 2020) polymerized electron-accepting DAAQ with electron-donating tetraformyltetrathiafulvalene to yield a donor–acceptor COF (TTF-COF1 in Table 1 entry 4). As a matter of fact, apart from DAAQ with substitution at 2,6-positions, amino groups in other positions were also confirmed to be able to construct anthraquinone-based COFs, such as 1,5-diaminoanthraquinone (AAn in Fig. 1A) and 1,5-diamino-4,8-dihydroxyanthraquinone (OH-AAn in Fig. 1A), and their twisted structures play great roles in regulating the morphology of materials.

Compared to β-ketoenamine or Schiff-base linkages, aromatic imide-based POPs are provided with excellent mechanical properties and high stability owing to the high-performance aromatic imide linkages. In addition, thanks to the redox-active carbonyl sites as well as strong π – π stacking interactions, aromatic polyimides are also promising organic electrode materials. In view of common aromatic anhydrides (e.g., pyromellitic dianhydride, 1,4,5,8-naphthalenetetracarboxylic dianhydride and 3,4,9,10-perylenetetracarboxylic dianhydride) bearing only linear structures, combining them with DAAQ gives rise to only linear polymers (Kim et al., 2022). The lack of multifunctional aromatic anhydride has been a major obstacle in regulating the structure–property relationship of polyimides. Recently, Yang et al. (Yang et al., 2022) designed an anhydride with C_3-symmetry (HATN-AP in Fig. 1B) and successfully prepared a polyimide COF (HATN-AQ-COF) containing anthraquinone, imide, and nitrogen-doping features simultaneously under solvothermal strong polar solvent conditions. By the way, owing to the low reversibility of imidization reaction, preparing polyimide COFs has been considered a big challenge (Zhang et al., 2020), and this further illustrates the ingenuity of their molecular design.

Covalent triazine frameworks (CTFs) are a class of important POPs for energy conversion and storage applications (Liu et al., 2019). Combining anthraquinone with CTF would expand the functions of the resulting materials. Generally, CTFs are gained from the trimerization of cyano groups, which requires harsh conditions and the usage of highly toxic cyanide. Ruoff *et al.* adopted a urea-

Table 1
Selected examples of the synthesis of anthraquinone-based POPs.

Entry	Polymers	Monomers	Reaction type	Synthesis conditions	POP type	Ref.
1	DAAQ-TFP	DAAQ, TFP	Aldoamine condensation	DMA, 6 M AcOH, 90 °C, 48 h	COF	(DeBlase et al., 2013)
2	TpOMe-DAQ	DAAQ, TpOMe	Aldoamine condensation	PTSA, grinding, then 90 °C, 48 h	COF	(Halder et al., 2018)
3	DAAQ-COF	DAAQ, BTA	Aldoamine condensation	DMA/TMB/AcOH, 120 °C, 72 h	COF	(Zhao et al., 2021)
4	TTF-COF1	DAAQ, TTF-fo	Aldoamine condensation	DMA/TMB/AcOH, 120 °C, 72 h	COF	(Li et al., 2020)
5	OH-AAn-COF	OH-AAn, TFP	Aldoamine condensation	Dioxane/o-DCB/AcOH, 120 °C, 72 h	COF	(Liu et al., 2021)
6	HATN-AQ-COF	DAAQ, HATN-AP	Imidization reaction	Mes/NMP/Isoquinoline, 180 °C, 120 h	COF	(Yang et al., 2022)
7	rCTF	DFAQ, M3	Urea-aldehyde condensation	DMSO, Cs_2CO_3, 130 °C, 48 h	CTF	(Buyukcakir et al., 2020)
8	AQ-CMP	DBrAQ, PTB	Suzuki – Miyaura coupling	$Pd(PPh_3)_4$, K_2CO_3, DMF, 150 °C, 48 h	CMP	(Zhong et al., 2021)
9	PBAQ-2	AQDB, TrBrB	Suzuki – Miyaura coupling	$Pd(PPh_3)_4$, K_2CO_3, DMF, 150 °C, 48 h	CMP	(Luo et al., 2022)
10	PBAQ-3	AQDB, TBrB	Suzuki – Miyaura coupling	$Pd(PPh_3)_4$, K_2CO_3, DMF, 150 °C, 48 h	CMP	(Luo et al., 2022)
11	PyAq	AQDB, TBrPy	Suzuki – Miyaura coupling	$Pd(PPh_3)_4$, K_2CO_3, DMF, 150 °C, 48 h	CMP	(Luo et al., 2021)
12	IEP-11-E	DBrAQ, TEB	Sonogashira coupling	$Pd(PPh_3)_4$, CuI, Et_3N, tol, 80 °C, 3 h 150 °C, 6 h for IEP-11-E, 12 h for IEP-11-E12	CMP	(Molina et al., 2019)
13	Py-A-CMP	DBrAQ, Py-T	Sonogashira coupling	$Pd(PPh_3)_4$, CuI, Et_3N, DMF, 110 °C, 72 h	CMP	(Mohamed et al., 2021)
14	TPE-A-CMP	DBrAQ, TPE-T	Sonogashira coupling	$Pd(PPh_3)_4$, CuI, Et_3N, DMF, 110 °C, 72 h	CMP	(Mohamed et al., 2021)
15	B-AQ	DEAQ, TBrDB	Sonogashira coupling	$Pd(PPh_3)_4$, CuI, Et_3N, THF, 75 °C, 72 h	CMP	(Zhou et al., 2023)
16	PAQTA	DBrAQ, TA	Buchwald–Hartwig Coupling	$Pd(dba)_2$/XPhos/NaOtBu/Tol., 110 °C, 72 h	CMP	(Liao et al., 2018)
17	PDAQ-BC	DAAQ, BC	Buchwald–Hartwig Coupling	$Pd(dba)_2$/XPhos/NaOtBu/Tol., 120 °C, 24 h	CMP	(Wu et al., 2019)
18	DA CMP3	AQCz	Oxidative coupling	$FeCl_3$, $CHCl_3$, 60 °C, 2 days	POP	(Zhi et al., 2019)
19	HAzo-POP	DAAQ, THB	Diazo-coupling	1) HCl, $NaNO_2$, 0 ~ 5 °C, 30 min; 2) Na_2CO_3, r.t., 12 h	POP	(Song et al., 2019)
20	2AQ	DHAQ, TFBQ	S_NAr	Et_3N, Dioxane, 120 °C, 72 h	POP	(Cao et al., 2022)
21	JUC-506	HHTP, TFAQ	S_NAr	Na_2CO_3, Mes/NMP, 160 °C, 72 h	COF	(Guan et al., 2019)
22	PTA-O26	DHAQ, TCT	S_NAr	Dioxane, reflux, 48 h	POP	(Wang et al., 2023)
23	PAT	DAAQ, TCT	S_NAr	Na_2CO_3, DMF, 100 °C, 20 h	COF	(Kang et al., 2018)
24	DAAQ – HCCP	DAAQ, HCCP	S_NAr	DMSO, Et_3N, sonication (160 W), 3 h.	COF	(Hu et al., 2021)
25	BQbTPL	HBB, BQ	Diels – Alder reaction	NaI, DMF, 130 °C, 7 days	CMP	(Ouyang et al., 2021)

aldehyde condensation method to construct an anthraquinone-based CTF (rCTF in Fig. 1C) with 2,6-diformylanthraquinone (DFAQ) and amidine dihydrochloride (M3 in Fig. 1C) as two key monomers (Buyukcakir et al., 2020). The mild temperature (130 °C) greatly avoids the further carbonization of resultant polymer.

2.2. Coupling reactions

Coupling reactions are classic organic reactions to construct rigid aromatic polymers. Bearing bromine atoms as good leaving group, aromatic bromine derivatives can undergo palladium-catalyzed coupling reactions with various functional groups, such as Suzuki-Miyaura cross-coupling (Fig. 2A) with boronic acid bis (pinacol) ester (Yu et al., 2022), Sonogashira cross-coupling (Fig. 2B) with terminal acetylene (Molina et al., 2019), and Buchwald–Hartwig coupling (Fig. 2C) with aromatic amine (Liao et al., 2018). Theoretically, there are two options for getting the desired anthraquinone-based POPs: one is to start with bromoanthraquinone as raw material, and the other is to use anthraquinone derivatives with other functional groups, meaning a wide range to select polymeric monomers. Table 1 (entry 8–––17) lists several examples of anthraquinone-based POPs prepared through these kinds of coupling reactions and Fig. 2F shows the reported corresponding monomers. According to the accessibility, solubility and reactivity of monomers, Buchwald–Hartwig coupling and Sonogashira cross-coupling are generally taking DAAQ and DBrAQ as the source of anthraquinone, respectively. For Sonogashira cross-coupling reaction, taking IEP-11 as example, Molina et al. (Molina et al., 2019) developed a novel synthesis method via miniemulsion polymerization followed by solvothermal treatment. Compared to polymer obtained from conventional polymerization, the S_{BET} of polymer prepared through this now approach had a tremendous increase from 609 m^2/g to 2200 m^2/g. For Suzuki-Miyaura cross-coupling, both DBrAQ and AQDB monomers have already been proven to work. Taking AQ-CMP (Table 1 entry 8 and PBAQ-2 Table 1 entry 9) as good examples, they have identical skeletal structure and could be gained from different monomers under same reaction conditions. However, the specific surface areas vary a lot (624 m^2/g for AQ-CMP and 91 m^2/g for PBAQ-2), indicating the importance of selecting polymeric monomers. Unlike condensation reactions bearing high reversibility which are meaningful to prepare COF materials, coupling reaction are usually less reversible. Therefore, it is tricky to gain crystalline COFs from coupling reactions, and the resultant polymers are mostly CMPs.

Additionally, three are other coupling reactions which could be utilized to prepare anthraquinone-based POPs, including oxidative coupling polymerization (Zhi et al., 2019; Deng et al., 2022) and diazo-coupling polymerization (Song et al., 2019). For oxidative coupling polymerization (e.g., DA CMP3 in Fig. 2D, (Zhi et al., 2019), anthraquinone was derivatized to aromatic amines and further oxidized by $FeCl_3$. Regard of diazo-coupling polymerization (Fig. 2E), aromatic amine was firstly transformed to diazo salt and then reacted with phenol derivative (Song et al., 2019). Considering the low regional selectivity and high complexity of these two coupling reactions, the structural regularity of corresponding POPs is not very good, resulting in wider pore size distributions or lower specific surface areas. Accordingly, these two coupling reactions have not received much attention.

2.3. Nucleophilic aromatic substitution reactions

Nucleophilic aromatic substitution (S_NAr) reactions have been widely utilized to construct diverse POPs bearing aromatic ether bonds, and the reactions between C—F bonds and hydroxyl groups are commonly used. For example, Cao et al. successfully prepared a quinonyl-rich POP (2AQ in Fig. 3A) via S_NAr reaction of 2,6-dihydroxyanthraquinone (DHAQ) and tetrafluoro-1,4-benzoquinone (TFBQ) (Cao et al., 2022). The strong electron-negative feature of benzoquinone makes fluorine atoms highly reactive with the nucleophilic hydroxyl groups in DHAQ. Given that anthraquinone is also highly electro-negative, the nucleophile and electrophile can interchange roles with anthraquinone-based

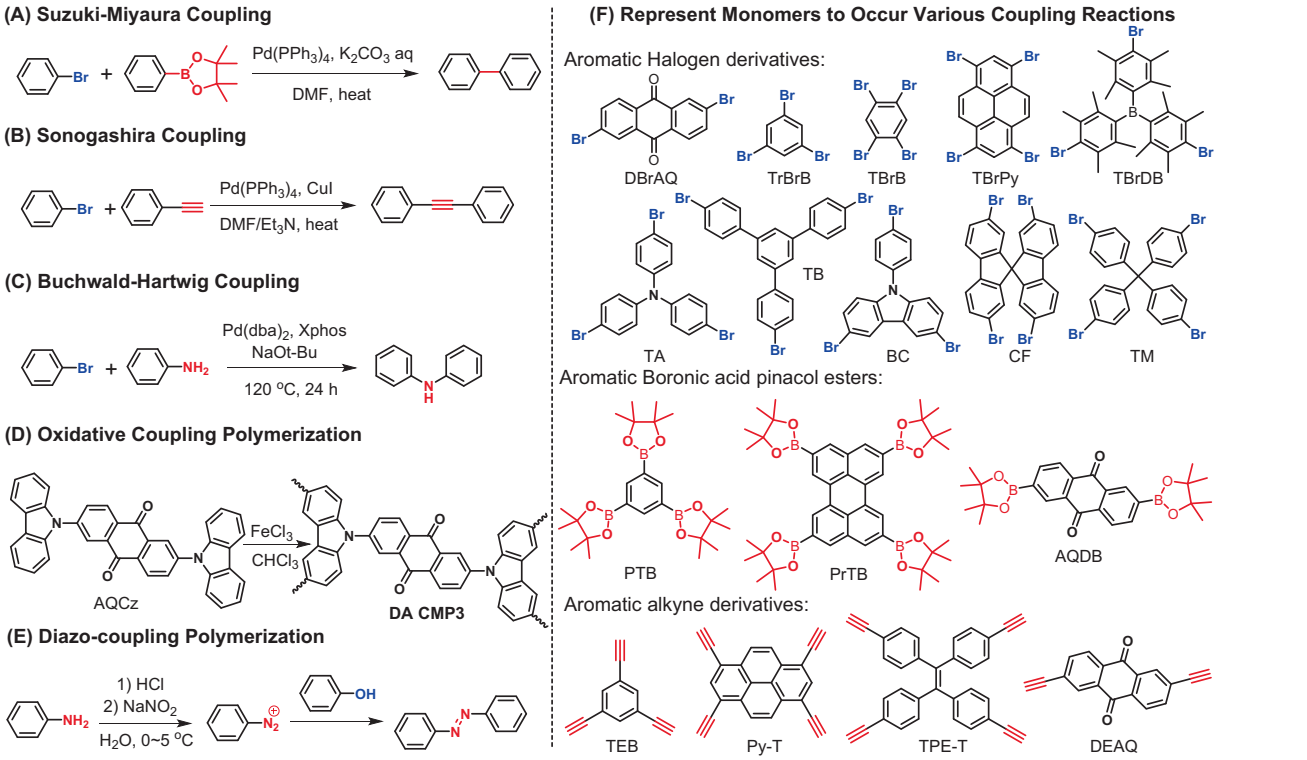

Fig. 2. Synthesis of anthraquinone-based porous organic polymers via various coupling reactions: (**A**) Suzuki-Miyaura cross-coupling, (B) Sonogashira cross-coupling, (C) Buchwald–Hartwig coupling, (D) oxidative coupling, (E) diazo-coupling, and (F) represent monomers bearing different functional groups.

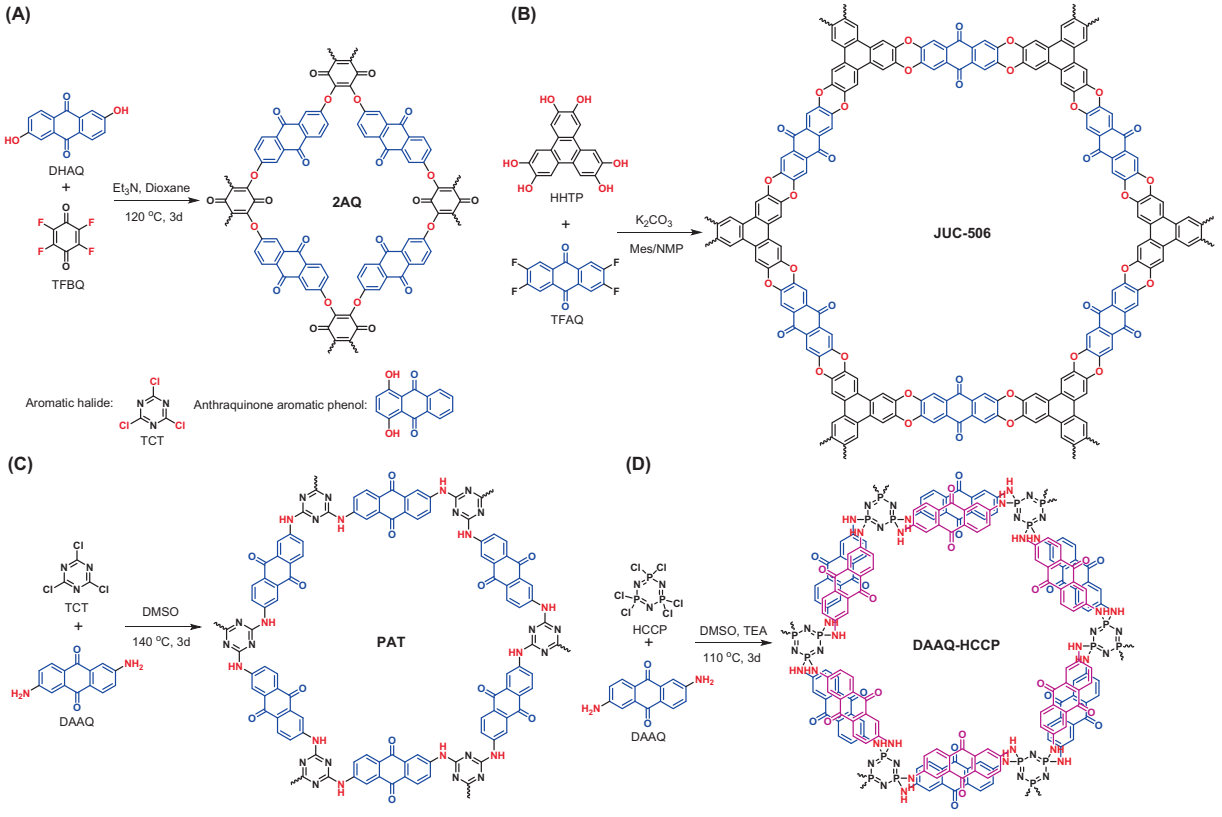

Fig. 3. Synthesis of anthraquinone-based porous organic polymers via nucleophilic aromatic substitution reaction.

monomer serving as electrophile. Hence, Guan *et al.* prepared a dioxin-linked COF (JUC-506 in Fig. 3B) bearing ladder-type structure from 2,3,6,7-tetrafluoroanthraquinone (TFAQ) and 2,3,6,7,10,11-hexahydroxytriphenylene (HHTP) (Guan et al., 2019). Owing to the high stability of aromatic ether linkages, the corresponding POPs behaved excellent chemical stability under various harsh conditions such as strong acid, strong base, and redox environments.

Except for C—F bond, C—Cl has been also demonstrated to build POPs by Wang et al. (Wang et al., 2023) with 2,4,6-trichloro-1,3,5-triazine (TCT in Fig. 3A) being selected as aromatic halide. Meanwhile, apart from DHAQ, 1,4-dihydroxyanthraquinone was also attempted, which gave a twisted structure owing to steric hindrance. The electro-negative capability of C—Cl bond is weaker than that of C—F bond, therefore aromatic chlorides are more likely to occur S_NAr reactions with aromatic amines which present more nucleophilic capability. Kang et al. (Kang et al., 2018) and Hu et al. (Hu et al., 2021) successfully prepared the corresponding POPs (PAT in Fig. 3C and DAAQ-HCCP in Fig. 3D) via S_NAr reactions of DAAQ with TCT and hexachlorocyclotriphosphazene (HCCP), respectively. By comparing these two types of S_NAr reactions (C—F with hydroxyl and C—Cl with amine), it is found that the strong electron-withdrawing quinone groups and nitrogen-doping subunits in aromatic halides are essential since they ensure the reaction activity of C—halogen bonds towards hydroxyl and amino groups.

2.4. Diels – Alder reaction

Diels-Alder reaction has been also proven to be a useful method to effectively construct functional POPs (Byun and Coskun 2018; Cao et al., 2022). However, the dienophiles are mainly furan derivatives. In 2017, we reported that hexakis(bromomethyl)benzene (HBB in Fig. 4) could occur Diels – Alder reaction with naphthoquinimide to yield a disk-shaped conjugated small molecule (Yao et al., 2017). The overall reaction undergoes at least three processes including the formation of dienophile intermediate ([6]radialene in Fig. 4), Diels – Alder reaction, and final aromatization. Based on these findings, Ouyang (Ouyang et al., 2021) designed and synthesized a fully-conjugated benzoanthraquinone-based CMP (BQbTPL in Fig. 4) via the Diels – Alder reaction of HBB and 1,4-benzoquinone (BQ). Several important factors play vital roles in the formation of this ladder-type CMP, such as good leaving group (Br atoms), high reactivity of the dienophile, and high aromatization tendency of intermediate.

3. Applications of anthraquinone-based POPs in electrochemical energy conversion and storage

3.1. Electrocatalysis

CO_2 electroreduction reaction (CO_2RR), as a very important way of converting electrical energy into chemical energy, is a very meaningful technology to pursuit carbon cycle. The specific process CO_2RR is pretty complex. In addition to being reduced to a variety of products such as CO, CH_3OH and CH_4, CO_2RR has to face the competition from hydrogen evolution reaction (HER). Especially for higher-value products (e.g., CH_4), the electroreduction usually involves multiple proton-coupled electron transfer processes (Wang et al., 2020). How to implement CO_2RR with high efficiency and high selectivity is a challenging task. Using "bottom-up" template-free synthesis strategy, Liu et al. (Liu et al., 2021) designed and prepared two anthraquinone-based COFs to explore this goal (AAn-COF and OH-AAn-COF Fig. 5). Owing to twisted structure stemming from substitutions at the carbonyl *ortho*-positions as well as polar hydroxyl functional groups, the obtained materials presented different assembly morphologies with nanofibers and hollow tubes for AAn-COF and OH-AAn-COF, respectively, which could be rationalized by nanosheet-based self-template mechanism and nanosheet-crimping mechanism. When post-modified with transition metals (Cu atoms showed the best performance), both the resultant nanostructures behaved high CO_2RR performances towards CH_4. For AAn-COF-Cu and OH-AAn-COF-Cu materials with flow cell, the faradaic-efficiency (FE_{CH4}) are 77% (−128.1 mA cm^{-2} at − 0.9 V) and 61% (−99.5 mA cm^{-2} at − 1.0 V), which nearly rank the highest ones among reported COF materials. The excellent chemical stability and sufficient active sites originating from periodic COF structure and special material morphology play indispensable roles in mass transfer and CO_2 activation, thus leading to enhanced performances. Moreover, the material morphology was observed to affect reduced products, while the nanofiber morphology was helpful for the formation of CH_4 and the hollow tube morphology had an effect on the production of ethylene. The anthraquinone-based support materials not only realize the efficient selective CO_2RR towards CH_4 but also provide a useful methodology to modulate the electrocatalytic performance by morphology-control.

In addition to being utilized as important supports for active materials, anthraquinone-based POPs could be also employed as important precursors to prepare useful substances for electrocatalysis since the abundant heteroatoms are very useful to yield heteroatom-rich porous materials (Bhambri et al., 2022). For example, graphitic nitrogen-doped porous carbons (Zhang et al., 2020; Zhang et al., 2020) and cobalt nanocrystals porous carbons (Wang et al., 2018) were successfully prepared though the pyrolysis of anthraquinone-based POPs independently or together with other components, and they have been demonstrated as important electrocatalysts for oxygen reduction reaction (ORR) and HER. In view of the anthraquinone subunits have been destroyed by pyrolysis processes, we don't put much effort into this kind of materials.

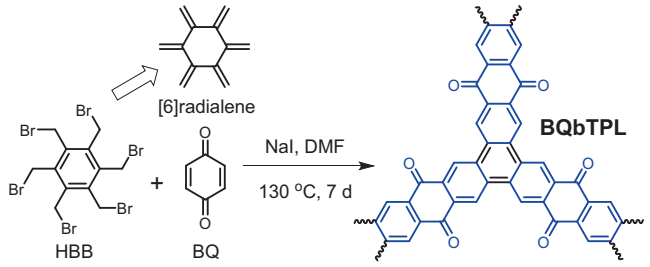

Fig. 4. Synthesis of ladder-type conjugated microporous polymer BQbTPL via Diels – Alder reaction.

3.2. Active components for batteries

The increasing energy crisis puts forward high requirements for novel energy storage materials and devices. Rechargeable batteries, such as lithium-ion batteries (LIBs), sodium-ion batteries (SIBs), and potassium-ion batteries (PIBs), and Zn-based aqueous batteries (ZABs) are excellent candidates (Xu et al., 2021; Yuan et al., 2022). The excellent redox characteristics of anthraquinone together with the advantages of POPs render anthraquinone-based POPs significant prospects to serve as active materials for various rechargeable batteries.

3.2.1. Lithium batteries

LIBs have been commercial for portable electronics and electric vehicles, and developing redox-active polymers are in consideration of the abundant sources, synthetic possibilities, lower-cost and sustainability of organic compounds. The carbonyl groups in anthraquinone-based POPs provide abundant active sites for elec-

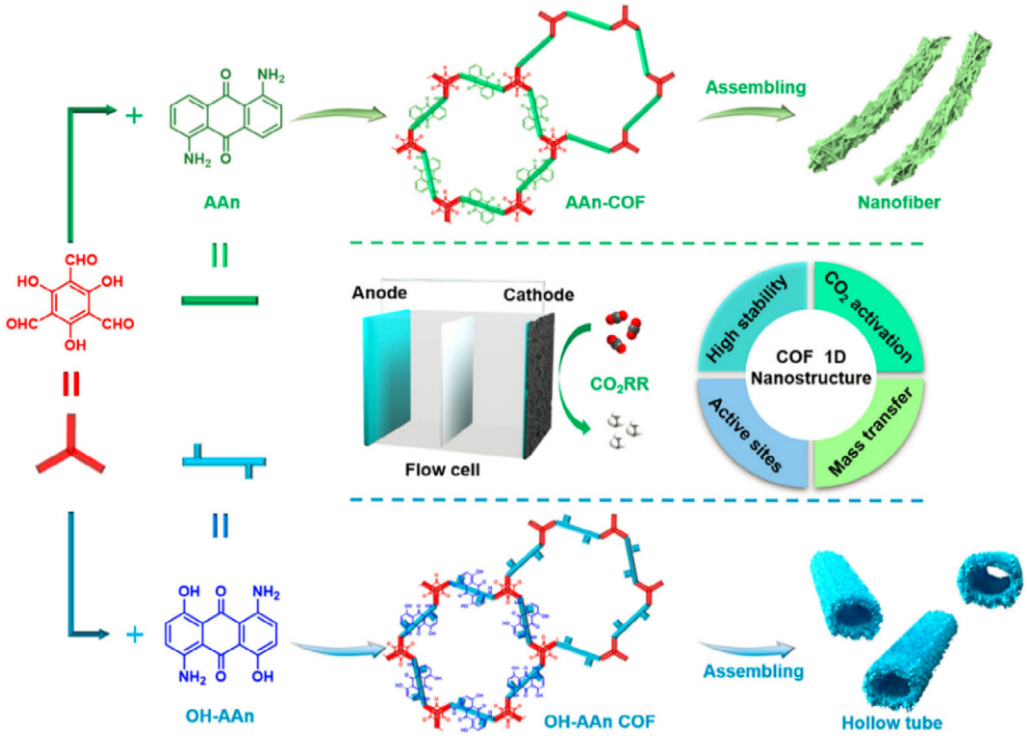

Fig. 5. Schematic illustration of the formation of anthraquinone-based nanofibers and hollow tubes and their applications in electrocatalytic CO_2RR (Liu et al., 2021).

trochemical lithiation and delithiation. When anthraquinone functions as the only electrochemically active unit, a very important class of POP are CMPs. Different from COFs which are crystalline, CMPs are generally a special subclass of amorphous polymers which combine expanded π-conjugation. There is evidence that it can be used as an electrode material for batteries because of its permanent microporosity and substantial active groups (Yu et al., 2022). As discussed previously in the synthesis section, Ouyang (Ouyang et al., 2021) adopted a miniemulsion-solvothermal method to prepare IEP-11-E. Actually, with the increasing time of solvothermal treatment, except for the increased specific surface area, the textural properties of CMPs were also improved with more mesoporosity. Moreover, the solution dispersibility was also enhanced, which was beneficial to prepare homogeneous electrodes bearing smooth surfaces. By virtue of these factors, the overall battery performances based on IEP-11-E12cathode material were greatly improved with excellent rate (50% capacity retention at 30C, detailed data are listed in Table 2 entry 1) and cycle performances (90% capacity retention after 5000 cycles at 2C). With Sonogashira cross-coupling reaction as an effective tool to build CMPs, pyrene and tetraphenylethene units were also incorporated into CMPs (Py-A-CMP and TPE-A-CMP in Table 2 entry 2 and entry 3, respectivly) (Mohamed et al., 2021), which have greater conjugation length and twisted structure. When acted as cathode active materials, they showed excellent initial discharge capacity. However, the cycle performance of Py-A-CMP electrode needs further improvement.

Theoretically, acetylene motifs do not play electroactive roles in the skeleton structures. Luo et al. (Luo et al., 2021) prepared PyAq CMP (Table 1 entry 11) combining pyrene and anthraquinone units via Suzuki – Miyaura coupling. Without acetylene functions, PyAq would have a higher theoretical battery capacity (175 mAh g^{-1}), nevertheless, a smaller pore-size (microporosity). As illustrated in Fig. 6A, high redox activity and reversibility of carbonyl groups render PyAq CMP simultaneously to show great potentials as active cathode materials for both LIB and PIB (PIB would be discussed in the following section). Encouragingly, the PyAq cathode for LIB presented a high specific capacity of 169 mAh g^{-1} (at 20 mA g^{-1}) which is basically close to its theoretical capacity, indicating ultrahigh carbonyl utilization (96.6%). The rate capability also performed very well (142 mAh g^{-1}) when the current density was elevated to 1A g^{-1}. To further improve the intrinsic conductivity of CMP materials, by virtue of the superior stability of ladder-type polymers meanwhile, Ouyang (Ouyang et al., 2021) designed a fully π-conjugated ladder-type CMP (BQbTPL in Fig. 4). When employed as active material for LIB cathode, the abundant quinone motifs and fused structure endows BQbTPL with high charge transport efficiency, thereby achieving superior rate capability as well as long-term cycle durability (94.8% capacity retention after 1500 cycles). Only anthraquinone functional groups are electroactive in the above discussed examples. In order to enhance the discharge capacity more effectively, it is a useful strategy to make every building unit electroactive as much as possible. Yang et al. (Yang et al., 2022) designed and fabricated a mesoporous polyimide-linked COF (HATN-AQ-COF) bearing multiple redox-active sites. As revealed in Fig. 6B, anthraquinone, imide, and hexaazatrinaphthalene subunits are all electroactive, therefore the theoretical capacity reaches up to 406 mAh/g. Together with the structural merits of inherent mesoporosity of 3.8 nm as well as high crystallinity, LIB with HATN-AQ-COF cathode presented high reversible capacity of 319 mAh/g and long-term cycle durability (80% after 3000 cycles), which ranks one of the best overall performances among reported COF-based electrodes.

Apart from the structural factors of POPs, the pattern of stacking or dispersion of active materials, the interactions with conductive materials, and the loading amount of active materials on electrodes would have decisive impacts on the battery performances. Considering the long eclipsed stacking mode in COFs might cause sluggish diffusion rate and low availability of active materials, Wang et al. (Wang et al., 2017) exfoliated the long stacking COFs into few-layer nanosheets via ball milling (Fig. 7A). The limited few layers would shorten the migration pathways and facilitate ionic/elec-

Table 2
Summary of the electrochemical performances of anthraquinone-based POP electrode materials for various batteries. (The meaning of capital abbreviations in the titles: A: Electrodes; B: Theoretical capacity; C: Initial discharge capacity; D: Rate capability at high C-rate; E: Potential window; F: Cycle performance; G: Battery type; AM: Active materials; CA: Conductive additives; BI: Binders.).

Entry	Materials	S_{BET} [m^2/g]	A AM: CA: BI	B [mAh/g]	C [mAh/g]	D [mAh/g]	E [V]	F	G	Ref.
1	IEP-11-E12	2200	50/40/10	149	104, 1C	46, 30C	1.5 ~ 3.5	90%, 5000, 2C	LIB	(Molina et al., 2019)
2	Py-A-CMP	123	40/50/10	181.20	196.6, 0.1C	40, 20C	1.7 ~ 3.0	61%, 400, 0.1C	LIB	(Mohamed et al., 2021)
3	TPE-A-CMP	514	40/50/10	162.74	164.7, 0.1C	19, 20C	1.8 ~ 3.0	99.3%, 400, 0.1C	LIB	(Mohamed et al., 2021)
4	PyAq	485	60/30/10	175	169, 20 mA g^{-1}	142, 1 A/g	1.5 ~ 3.0	79.6%, 4000, 1 A/g	LIB	(Luo et al., 2021)
5	PyAq	485	60/30/10	175	143, 20 mA g^{-1}	85, 1 A/g	1.5 ~ 3.0	93%, 800, 100 mA g^{-1}	PIB	(Luo et al., 2021)
6	BQbTPL	215	50/40/10	262.7	140, 0.2 A g^{-1}	97.3, 1 A/g	1.0 ~ 3.5	94.8%, 1500, 1 A/g	LIB	(Ouyang et al., 2021)
7	HATN-AQ-COF	725	50/40/10	406	319, 0.5C	226, 10C	1.2 ~ 3.9	80%, 3000, 10C	LIB	(Yang et al., 2022)
8	DAAQ-ECOF	216	60/30/10	153	145, 20 mA g^{-1}	76, 3 A/g	1.5 ~ 4.0	98%, 1800, 20 mA g^{-1}	LIB	(Wang et al., 2017)
9	IEP-11-S5R5	960	80/20/0	149	147, 1C	0,8[a], 10C	1.5 ~ 3.5	93%, 760, 1C	LIB	(Molina et al., 2020)
10	AQ-COF@CNTs	905	60/30/10	153	144, 50 mA g^{-1}	69, 10 A/g	1.25 ~ 3.5	100%, 3000, 0.25 A/g	LIB	(Amin et al., 2020)
11	DAAQ-COF	73.1	60/30/10	692	1698, 1 A/g	350, 5 A/g	0.01 ~ 3.0	46.3%, 500, 1A/g	LIB	(Zhao et al., 2021)
12	rCTF	766	90/5/5	1198	1750, 0.05C	420, 20C	0.005 ~ 3.0	68%, 1500, 0.5C	LIB	(Buyukcakir et al., 2020)
13	PAT	140	60/25/15	1450	2550, 0.2 mA g^{-1}	540, 2 A/g	0.01 ~ 3.0	69%, 400, 200 mA g^{-1}	LIB	(Kang et al., 2018)
14	Co@2AQ-MnO_2	/	60/30/10	1329.9	1346.2, 0.1 A/g	511.9, 2 A/g	0 ~ 3.0	114%, 200, 0.25 A/g	LIB	(Cao et al., 2022)
15	DAAQ-TFP	/	60/30/10	470	420, 0.1 A/g	198, 5 A/g	0.05 ~ 3.0	99%, 10000, 5 A/g	SIB	(Gu et al., 2019)
16	PBAQ-3	420	60/30/10	220	200, 0.05 A/g	105, 200C	0.9 ~ 2.3	83.1%, 40000, 3 A/g	SIB	(Luo et al., 2022)
17	DAAQ-TFP@CNT	644.8	60/30/10	153	157.7, 0.1 A/g	111.2, 1 A/g	0.8 ~ 2.8	77.6%, 500, 0.5 A/g	PIB	(Duan et al., 2022)
18	AQ-CMP	624	60/30/10	209.4	202, 2 A/g	115, 20 A/g	−1.1 ~ − 0.1	100%, 60000, 20C	RAB	(Zhong et al., 2021)
19	IEP-11||$Ni(OH)_2$	738	90/5/5	165	150, 1C	72, 1000C	−1.2 ~ 0	75%, 22730, 20C	ARB	(Grieco et al., 2022)
20	PVC-Zn-AAn-COF@Zn||MnO_2	279	70/20/10	308	217.2@0.2 A/g	119.3@2 A/g	0.8 ~ 1.8	76.2%, 1000, 2 A/g	ZAB	(Guo et al., 2022)

[a] The measurement unit of rate capability for IEP-11-S5R5 is 0.8 mAh cm^{-2}.

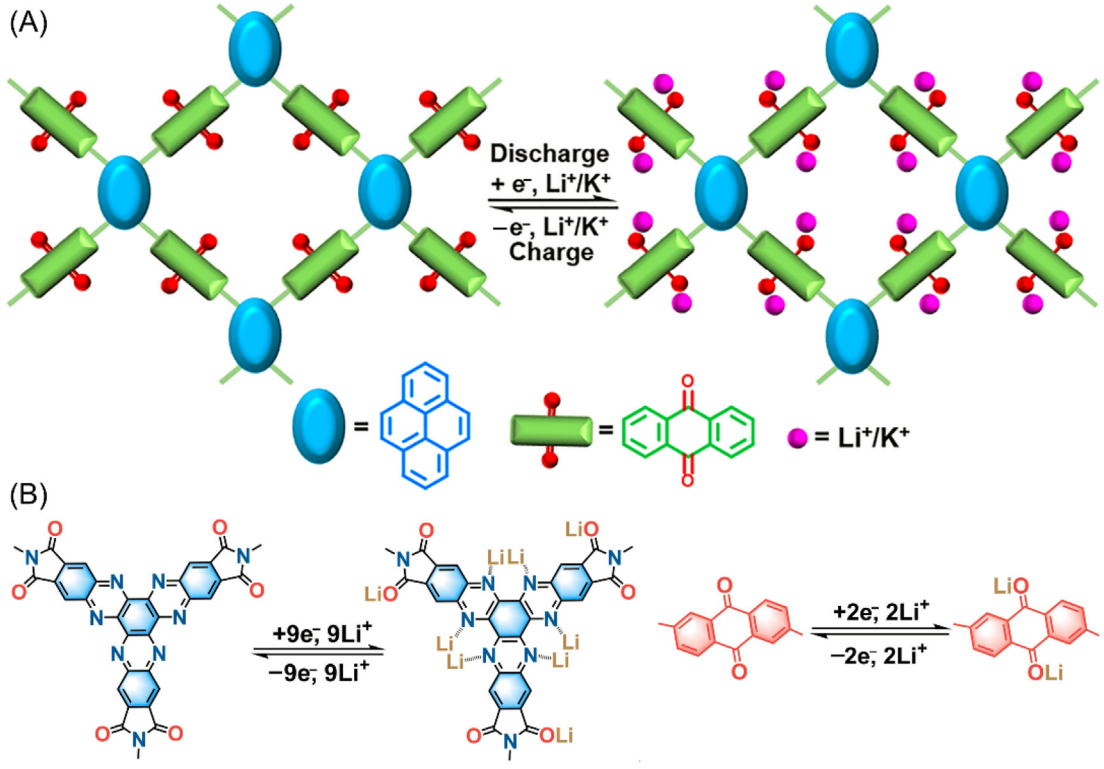

Fig. 6. (**A**) Schematic representation of the Li+/K + ions storage of PyAq (Luo et al., 2021). (**B**) Schematic representation of the potential lithium binding sites in HATN-AQ-COF (Yang et al., 2022).

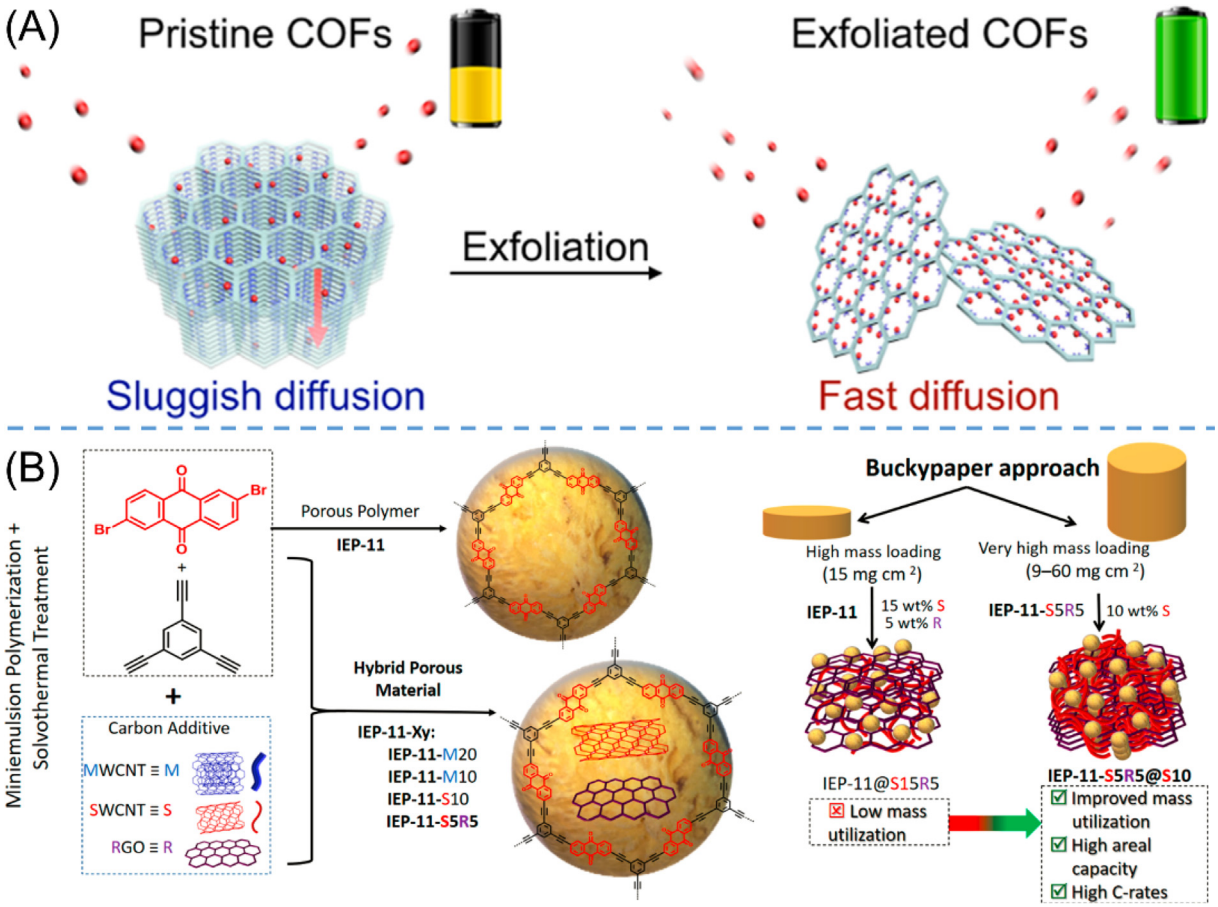

Fig. 7. (**A**) Schematic diagram for the exfoliation of long-range stacking COFs into few-layer exfoliated COFs serving as cathode material for LIB (Wang et al., 2017). (**B**) Schematic diagram of the synthesis IEP-11-Xy hybrid porous materials as well as the preparation process to gain high-mass-loading electrodes by buckypaper approach (Molina et al., 2020).

tronic diffusion, leading to higher utilization efficiency (94.7%) of COFs as well as faster kinetics (DAAQ-ECOF in Table 2 entry 8). Except simply focusing on the polymers, the characteristics of porosity and high specific surface areas of anthraquinone-based POPs endow them with great potentials to integrate with other substances (e.g., nano-carbon materials), giving rise to more smart materials. In 2020, Molina et al. (Molina et al., 2020) fabricated a series IEP-11-Xy hybrid porous materials through the preparation of IEP-11 CMP in the presence of different carbon nanostructures, and then the corresponding composite materials were further assembled into self-supported buckypaper electrodes (Fig. 7B). This innovative electrode preparation method not only improved the interactions between POPs and conductive materials, but also greatly increased the mass loading (60 mg cm^{-2}) of active materials on the electrode. By condition optimizations, the buckypaper cathode electrode based on IEP-11-S5R5@S10 showed the best performances with excellent electrochemical performances (detailed data see Table 2 entry 9), and the gravimetric capacity (83.7 mAh $g^{-1}_{electrode}$) and areal capacity (6.3 mAh cm^{-2}) were the best reported values of organic electrode materials. Similarly, Amin et al. (Amin et al., 2020) adopted an approach of in situ polymerization with carbon nanotubes to improve the conductivity, and the electrochemical properties was also enhanced (AQ-COF@CNTs in Table 2 entry 10).

Actually, in addition to being positive active materials, anthraquinone-based POPs have been also investigated as anode active materials, which also obtains good battery performances. For instance, anthraquinone-based POPs (e.g., DAAQ-COF, rCTF, PAT in Table 2 entry 11–––13) and related hybrid materials (Co@2AQ-MnO_2 in Table 2 entry 14) all behave superior properties. Nonetheless, the contribution of anthraquinone structural unit to battery specific capacity is not the main factor since almost all the conjugate units would make contributions, such as anthraquinone, triazine, and benzene (Buyukcakir et al., 2020). These polymers do not exhibit the unique advantages of anthraquinone building blocks, therefore we do not discuss them in detail. By the way, anthraquinone-based COF can also play other roles. Guo et al. (Guo et al., 2022) added a small amount (1 wt%) of OH-AAn-COF as a binder microadditive in lithium-sulfur battery. The hollow tube of OH-AAn-COF not only strengthened the necessary properties of the binder, but also played key role in spontaneous immobilization and catalytic conversion of lithium polysulfides, leading to doubly enhanced reversible capacity. This study opens a new avenue for the applications of COFs in the field of energy storage.

3.2.2. Na- and K-ion batteries

SIB and PIBs, two kinds of alternative battery techniques to replace LIBs, have attracted considerable attention owing to the merits of low potentials (M^+/M, M = Na, K), easy resource availability, and particularly the higher abundances of Na and K elements on the earth (Wang and Zhang 2018). Nevertheless, the larger ionic radiuses of Na^+ and K^+ would generally cause slow diffusion kinetics and serious structural deterioration of electrode materials upon repeated charging-discharging processes, thus leading to low capacity and poor cycle stability. The high surface area and inher-

ent insolubility of redox-active POPs provide an effective approach to address this issue. As mentioned above, PyAq is endowed with high activity for LIB and PIB simultaneously (Luo et al., 2021). The PIB performances were pretty good containing high reversible capacity, good rate capability, and good cycling stability (Table 2 entry 5). Doubtlessly, the PIB performances were slightly reduced in comparison to those of PyAq-based LIB. Except for the ionic radius factor, much thicker solid electrolyte interphase (SEI) film and higher electrolyte concentration were also put forward to explain the decreased properties. With smaller building unit so as to produce more theoretical capacity, Luo et al. (Luo et al., 2022) investigated the effect of linking patterns of building blocks on the electrochemical performances. Three topological structures, including 1,4-, 1,3,5- and 1,2,4,5- linkage on benzene connecting with anthraquinone, were designed and prepared. It is found that increasing the number of linkages on benzene would not only enhance the specific surface area but also improve the conjugation length of resultant polymers. Therefore, PBAQ-3 with 1,2,4,5-linkage presented the best performances (Table 2 entry 16).

Remarkably, there are some materials (e.g., DAAQ-TFP) could be suitable for multiple kinds of metal-ion batteries. In addition to serving as cathode active materials for LIBs (Table 2 entry 8 and entry 10), DAAQ-TFP also exhibits high activities for SIBs and PIBs. Gu et al. (Gu et al., 2019) paid close attention to the radical intermediates during the charging and discharging of SIB. In order to balance the reactivity, kinetics and stability of radical intermediates, they stripped DAAQ-TFP into various samples bearing different stacking thickness (including 4–––12 nm, 50–––85 nm, 100–––180 nm and 100–––250 nm) via different exfoliation processes (e.g., ball milling and solvent stripping). With comprehensive techniques, it is found that the C-O· and α-C radical intermediates play subtle roles in the Na^+ insertion/extraction processes (Fig. 8A), and the reduced thickness is beneficial for its contributive capacity as well as the stabilization of radical intermediates. The anode electrode with the thinnest stacking thickness (4–––12 nm) exhibited the highest specific capacity, optimal rate capability, and best perfect long-term cycle life (99% capacity retention after 10 000 cycles at high C-rate of 5 A/g). Duan et al. (Duan et al., 2022) adopted an in situ polymerization method to integrate a few-layered DAAQ-COF to carboxylated carbon nanotubes (DAAQ-COF@CNT in Table 2 entry 17), in which the few-layered DAAQ-COF acted as cathode active materials would provide more exposed active sites and shorten ion/electron diffusion length and the CNT nanofiber could improve electrical conductivity and mechanical properties to prevent large volume changes. Owing to the above-mentioned merits, when utilized as cathode active material for PIBs, DAAQ-COF@CNT presented enhanced performances than those of bare DAAQ-COF. The specific mechanism for K^+ storage was also rationally speculated. As represented in Fig. 8B, unlike as anode materials in which all the carbonyl groups are electroactive, only the carbonyl groups in anthraquinone units play active roles when used as cathode material. For one repeating six-membered ring, each six K^+ is accommodated step-by-step. The successes of these examples offer new design strategies for the fabrication of high-performance organic electrode materials for SIBs and PIBs.

3.2.3. Other batteries

The metal-ion batteries discussed above are primarily based on organic solvents as supporting electrolytes. In fact, aqueous rechargeable batteries could also provide attractive competitiveness in term of their intrinsic advantages of cost effectiveness, low volatility, low toxicity, and non-flammability of water-based electrolytes. However, the drawbacks of low energy density, high self-discharge and short service life limit their practical large-scale applications. Anthraquinone-based POPs could play positive

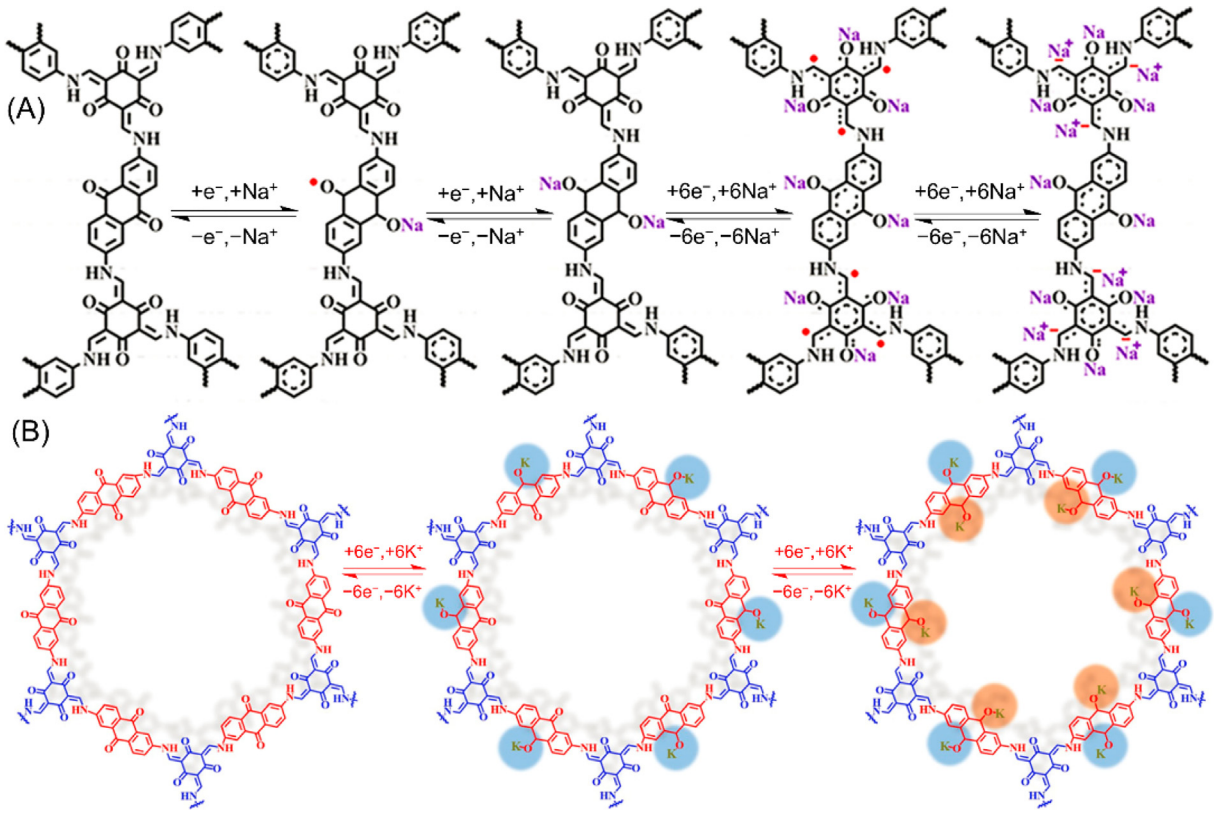

Fig. 8. (**A**) Redox sodiation mechanism of DAAQ-COF anode with the stacking thickness of 4–––12 nm (Gu et al., 2019). (**B**) K^+ storage mechanism of DAAQ-COF@CNT for PIB cathode during cycling processes (Duan et al., 2022).

roles in alleviating these restrictions. For example, as outlined in Table 2 entry 18–––20, AQ-CMP (Zhong et al., 2021), IEP-11 (Grieco et al., 2022), and Zn-AAn-COF (Guo et al., 2022) were assembled into the anodes of various aqueous rechargeable batteries such as rechargeable air batteries (RABs), alkaline rechargeable batteries (ARBs) and Zn-based aqueous batteries (ZABs), in which the POPs in the anodes served as active material, active material and support material, respectively. The performances of corresponding batteries were superior to their linear counterparts and other reported anode composite materials.

By comparing several types of batteries discussed above, from the POPs point of view, there are several common characteristics that contribute to the improvement of battery performances. Firstly, the intralayer π-conjugated skeletons or few-layer stacking structure greatly facilitate charge transfer. Secondly, the nanoscale open channels provide convenient and short diffusion avenues for mass transport. Thirdly, the porous structures supply sufficient space for electrolytes to contact with redox sites. Finally, the rigid polymer backbones together with highly crosslinked network structures ensure that POPs are impermeable to dissolution, which results in high cycle stability. The synergistic effect of these factors would play pivotal roles in improving material utilization efficiency as well as discharge capacity, enhancing rate performance, and prolonging the service life of batteries.

3.3. Supercapacitors

Supercapacitors, which could be also called ultracapacitors or pseudocapacitors, are considered as another class of promising devices for energy storage owing to their good energy density (E_d), high power density (P_d) and long-term cycle stability. The characteristics of anthraquinone-based POPs, including low cost, sustainable availability, excellent redox electrochemistry, good structural tunability and high environmental stability, make them desirable materials for supercapacitors (Ega and Srinivasan 2022).

3.3.1. Polymer materials engineering

The first anthraquinone-based POP for supercapacitor (DAAQ-TFP in Table 3 entry 1) was reported by DeBlase (DeBlase et al., 2013) in 2013. The high specific surface area and the reversible electrochemical processes render DAAQ-TFP capable of capacitive energy storage. Two charge storage mechanism, including electrical double-layer capacitance (EDLC) and surface-bound Faradaic capacitance (pseudocapacitance), were both found to contribute the final capacitance. Besides, except for conductivity and accessibility of materials, the EDLC and the pseudocapacitance are more directly related to the electroactive surface area and the nature of redox process, respectively. Owing to the polycrystalline structure as well as the random orientation of DAAQ-TFP COF particles, the utilization rate of active materials was pretty low (2.5%). He et al. (He et al., 2022) regulated the morphologies of polymers by modulating polymerized conditions, thus improving the material utilization rates. In their study, solvent effects and pre-polymerization methods were adopted to manipulate the different growth direction of COFs (Fig. 9A). Consequently, two well-crystalline COFs bearing different morphologies, that is flake-flower (COFs-F) and rod-flower (COFs-R), were prepared. Despite the slightly decreased specific surface areas, the unique morphologies make COFs-F and COFs-R have more available redox active sites and more regular pores, leading to higher specific capacitance of 407.7F/g and 486.3F/g for COFs-F and COFs-R, respectively. Moreover, kinetic analysis further revealed that the capacitance contribution rate of COFs-R reaches up to 95.3% (at 100 mV s^{-1}). On the contrary, Geng et al. (Geng et al., 2022) improved the performances of COF materials via post-modification method (DAAQ–TFP–COF in Table 3 entry 4). A pinpoint surgery was conducted on the β-ketoenamine linkages, in which the N—H bonds were deprotonated into N^- anions in high-pH aqueous electrolyte (pH = 11.5). Following this useful method, DAAQ–TFP–COF was assembled into an aqueous Li-ion capacitor and presented enhanced performances. These examples provide innovative strategies for improving the electrochemical performances of supercapacitors through front control and post-modification.

Polyaniline nanostructures have proved to be good polymer-based electrode materials for supercapacitors. Nonetheless, the swelling and shrinkage during charge–discharge cycles stemming from linear macromolecular structures leads to decreased cycle stability. With Buchwald–Hartwig coupling reactions as effective approach to yield C—N bonds, Liao (Liao et al., 2018) prepared a series of anthraquinonylamine-based POPs. Benefiting from the excellent redox properties of anthraquinone and aromatic amines, the POPs exhibited superior electrochemical energy storage features. Among various building blocks (e.g., triphenylbenzene, carbazole, tetraphenylmethane, spirobifluorene, and triphenylamine), the strongest electron donor triphenylamine standed out and the corresponding CMP (PAQTA in Fig. 9B and Table 3 entry 5) exhibited an exceptional specific capacity of 576F/g. Upon assembling into asymmetric two-electrode supercapacitors, the device based on PAQTA showed a wide working potential window (0–1.6 V), high energy density (60 Wh kg^{-1}), and high power density (1300 W kg^{-1}). By virtue of the donor–acceptor strategy to facilitate charge transfer, Li et al. (Li et al., 2020) fabricated another donor–acceptor COF (TTF-COF1 in Fig. 9C and Table 3 entry 6) in which tetrathiafulvalene served as strong donor unit, and the specific capacitance was further elevated to 752F/g. In order to enhance the electrical conductivity, Zhou (Zhou et al., 2018), Yan (Yan et al., 2019), and Song (Song et al., 2021) prepared diverse heteroatom-doped porous carbon materials (Table 3 entry 7–9) using pyrolysis method with anthraquinone-based POPs as precursors. The specific capacitance and the cycle performance are greatly enhanced, however, the basic structure of anthraquinone is destroyed as mentioned above, thus they would not be discussed in detail.

3.3.2. Electrode engineering

As mentioned above, whether it is EDLC or pseudocapacitance, they are closely related to the electrical conductivity of materials as well as the electrochemical accessibility to active sites. The low conductivity of POPs and the poor accessibility of active sites are generally the main reasons for low electrochemical performances. Therefore, improving the conductivity and the accessibility is very valuable topic. Electrode engineering would be beneficial to ameliorate these problems. For example, a certain amount of conductive materials (e.g., acetylene black and graphite) as well as binder (e.g., PVDF) are usually added to the active materials to improve the conductivity of active materials and the contact with electrodes. However, the poor electrical contact to insoluble COF samples is still a major problem. This section will briefly introduce several methodologies to improve the electrical conductivity and electrochemical utilization of materials.

DeBlase et al. (DeBlase et al., 2015) used gold, which has good electrical conductivity, as the working electrode. In their study, an in-situ polymerization of DAAQ-TFP COF was conducted in the presence of Au substrates, and TFP monomer was slowly introduced to DAAQ solution during the preparation process so as to form oriented thin films (Fig. 10A). The resultant COF thin film-modified Au was directly utilized as working electrode for capacitance test. This particular electrode preparation method would make more facilitated electrical conductivity not only between active material and electrode but also between different layers of COF crystallites. As a result, 80–––99% of the anthraquinone motifs are electrochemically accessed depending on the thickness of thin

Table 3
Summary of the electrochemical characteristics of anthraquinone-based POPs for supercapacitors (The meanings of capital abbreviations in the titles: A: Conductive materials; B: Electrolyte; C: Work potential window; D: Specific capacitance; E: Energy density; F: Power density; G: Cycle performance).

Entry	Materials	S_{BET} [m^2/g]	A*1	B	C [V]	D*2 [F/g], Current density	E [Wh kg^{-1}]	F [W kg^{-1}]	G*3	Ref.
1	DAAQ-TFP	1124	AB	1 M H_2SO_4	−0.3 ~ 0.3	48, 0.1 A/g	/	/	83%, 5000, 0.1 A/g	(DeBlase et al., 2013)
2	COFs-F	988.29	AB	1 M KOH	−0.9 ~ − 0.2	407.7, 0.5 A/g	/	/	86%, 10000, 0.5 A/g	(He et al., 2022)
3	COFs-R	713.51	AB	1 M KOH	−0.9 ~ − 0.2	486.3, 0.5 A/g	/	/	93.2%, 10000, 0.5 A/g	(He et al., 2022)
4	DAAQ-TFP-COF	783	CP	2 M LiCl	−1.0 ~ − 0.4	224, 0.1 A/g	/	4000	67%, 10000, 2 A/g	(Geng et al., 2022)
5	PAQTA	331	AB	0.5 M H_2SO_4	0.2 ~ 0.8	576, 1 A/g	60	1300	80%, 6000, 2 A/g	(Liao et al., 2018)
6	TTF-COF1	729	AB	3 M KOH	0 ~ 0.5	752, 1 A/g	57	858	90%, 10000, 1 A/g	(Li et al., 2020)
7	HPCF@500	838	AB	1 M H_2SO_4	−0.7 ~ 0.5	480, 0.1 A/g	/	/	100%, 10000, 5 A/g	(Zhou et al., 2018)
8	ONC-T1-850	1518	/	1 M H_2SO_4	0 ~ 0.6	1711, 1 A/g	/	/	100.5%, 10000, 10 A/g	(Yan et al., 2019)
9	TT-DQ	1993	Graphite	1 M H_2SO_4	0 ~ 1.0	468, 1 A/g	128	327	93.1%, 1000000, 1 A/g	(Song et al., 2021)
10	DAAQ-TFP	/	Au	1 M H_2SO_4	−0.3 ~ 0.25	3.0 mF cm^{-2}, 150 μA cm^{-2}	/	/	93%, 5000, 80C	(DeBlase et al., 2015)
11	PEDOT-modified DAAQ-TFP	6 cm^2 cm^{-2}	Au, PEDOT	0.5 M H_2SO_4	−0.9 ~ 0	350F cm^{-3}, 10C	/	/	100%, 10000, 100C	(Mulzer et al., 2016)
12	PEDOT@AQ-COF	131	PEDOT	1 M H_2SO_4	−0.2 ~ 0.6	1663, 1 A/g	/	/	118%, 10000, 50 A/g	(Wu et al., 2019)
13	DAAQ-TFP/GA	425.3	GA	1 M H_2SO_4	−0.5 ~ 0.5	378, 1 A/g	30.5	700	87.8%, 20000, 15 A/g	(An et al., 2021)
14	$COF_{DAAQ\ BTA}$-3DG	/	3DG	1 M KOH	−1.05 ~ − 0.4	31.7 mF cm^{-2}, 0.5 mA cm^{-2}	/	/	24%, 2000,0.5 mA cm^{-2}	(Zha et al., 2015)
15	TpOMe-DAQ	1531	/	3 M H_2SO_4	−0.5 ~ 0.5	1600 mF cm^{-2}, 3.3 mA cm^{-2}	2.9 μWh cm^{-2}	61.8 μW cm^{-2}	>120%, 100000,10 mA cm^{-2}	(Halder et al., 2018)
16	Dq_1Da_1Tp	804	/	1 M H_2SO_4	−0.7 ~ 0.3	111, 1.56 mA cm^{-2}	0.3 μWh cm^{-2}	960 μW cm^{-2}	78%, 7000, 0.39 mA cm^{-2}	(Khayum et al., 2018)
17	DqDaTp-CNF	532	CNF	1 M H_2SO_4	−0.5 ~ 0.5	364 mF cm^{-2},0.25 mA cm^{-2}	5.8 μWh cm^{-2}	125 μW cm^{-2}	76%, 4500, 5 mA cm^{-2}	(Mohammed et al., 2019)
18	c-CNT@COF-3	331.8	c-CNT	0.5 M H_2SO_4	−0.3 ~ 0.3	123.2 mF cm^{-2}, 0.2 mA cm^{-2}	30.7 μWh cm^{-2}	591.9 μW cm^{-2}	94.3%, 10000,10 mA cm^{-2}	(Kong et al., 2021)
19	AC-COFs	/	CNTF	1 M H_2SO_4	−0.4 ~ 0.5	1034 mF cm^{-2}, 1 mA cm^{-2}	194.64 μWh cm^{-2}	380 μW cm^{-2}	98%, 20000,10 mA cm^{-2}	(He et al., 2022)
20	COF@OHP	167	CNTF	1 M H_3PO_4	−0.4 ~ 0.4	249, 0.2 mA cm^{-2}	/	/	80%, 10000, 0.8 mA	(Xu et al., 2020)
21	COF@rGO-2	432	rGO	1 M H_2SO_4	−0.3 ~ 0.7	451.96, 0.2 A/g	44.22	9998	94.02%, 10000, /	(Yao et al., 2022)
22	CMAP@A4G	498	AG	1 M H_2SO_4	0 ~ 1.0	751, 1.0 A/g	76.6	27,634	95%, 20000, 10 A/g	(Jang et al., 2022)
23	PDT/$Ti_3C_2T_x$	/	$Ti_3C_2T_x$	0.5 M H_2SO_4	0 ~ 0.6	284 mF cm^{-2}, 0.5 mA cm^{-2}	24 mWh cm^{-3}	502 mW cm^{-3}	100%, 10000, /	(Wu et al., 2019)

*1The meanings of abbreviations in the conductive materials column: AB: acetylene black; CP: carbon paper; GA: 3D graphene aerogel; 3DG: 3D graphene, CNF: carbon nanofibers; c-CNT: carboxylated carbon nanotube; CNTF: carbon nanotube film; rGO: reduced graphene oxide; AG: activated graphene.
*2The specific capacitance was gained from three-electrode cell configuration.
*3The cycle performances of TTF-COF1, Dq_1Da_1Tp, and COF@rGO-2 are based on asymmetric/symmetric supercapacitor.

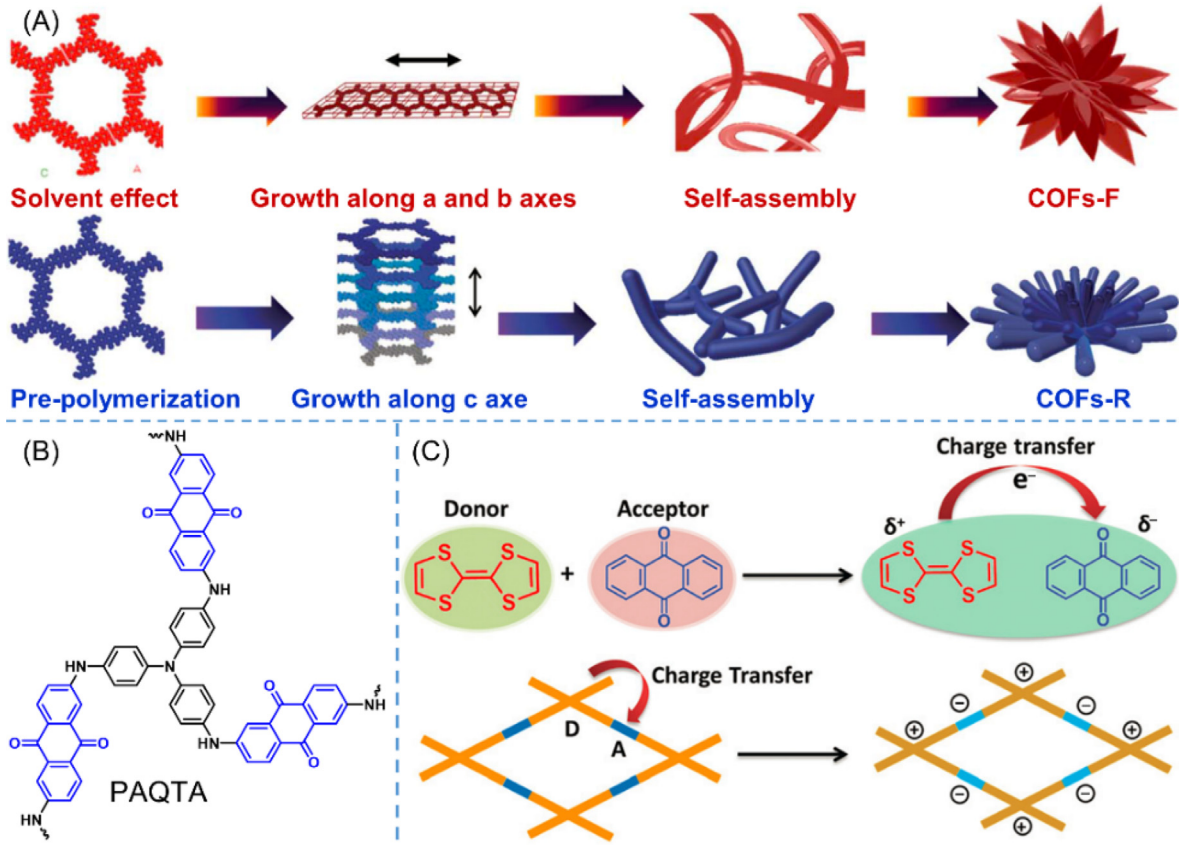

Fig. 9. (**A**) Schematic illustration of the proposed self-assembly mechanism of flake flowers (COFs-F) and rod flowers (He et al., 2022). (**B**) Chemical structure of PAQTA. (**C**) Schematic diagram of the charge transfer in tetrathiafulvalene and anthraquinone-based donor–acceptor COF (Li et al., 2020).

films (<200 nm), and the specific capacitance (3.0 mF cm^{-2}) is almost an order of magnitude enhancement over the conventional COF microcrystalline powder (0.40 mF cm^{-2}). Although the electrochemical performance is enhanced by using gold electrode, the adsorption mode as well as modest conductivity determine that the active material can only behave well at thin film thickness and slow charge–discharge rate. The same group addressed this limitation by further introducing conductive polymer with high electron mobility (Mulzer et al., 2016). 3,4-Ethylenedioxythiophene (EDOT) in CH_3CN solution was electropolymerized within the pores of DAAQ-TFP COF (Fig. 10B, left), and the electrical conductivity was drastically enhanced. As a consequence, the PEDOT-modified COF film working electrode performed nearly quantitative utilization rate of their redox-active groups and maintained high performances at thick film (1 μm) and fast charging rates (up to 1600C). The corresponding volumetric energy density and volumetric power density increased 30-fold and 12-fold, respectively, in comparison to the as-synthesized COF film.

To overcome the tedious processes of electrode preparation including COF-modified Au precursor and electropolymerization, Wu (Wu et al., 2019) developed an in situ solid-state polymerization approach. AQ-COF (the same skeleton structure with DAAQ-TFP COF) was firstly prepared by conventional solvothermal method, and the resulting polymer was subsequently carried out in situ solid-state polymerization with 2,5-dibromo-3,4-ethylene dioxythiophene. The solvent- and catalyst-free polymerization mode could tightly confine the conductive PEDOT chain within the nanochannels of AQ-COF, leading to an electron highway upon external electrochemical stimulus (Fig. 10B, right). Therefore, the PEDOT@AQ-COF nanocomposite showed billion-fold enhanced electrical conductivity (1.1 S cm^{-1}) and remarkably improved capacitance performances (Table 3 entry 12).

Alternatively, An et al. (An et al., 2021) improved material conductivity and active site utilization by the introduction of 3D graphene aerogels. Specifically, a binder-free DAAQ-COFs/GA composite electrode (the chemical structure of DAAQ-COF is the same with DAAQ-TFP COF) was fabricated by an electrostatic self-assembly of cationic surfactant modified-DAAQ-COF and negatively charged graphene oxide nanosheets under hydrothermal conditions (Fig. 10C). The hierarchical porous structure of COF together with aerogel and the rapid redox reactions of anthraquinone are conducive to enhance the utilization rate of active sites and to facilitate the ion/electron transfers. Accordingly, DAAQ-COFs/GA electrode presented not only high specific capacitance (378F/g at 1 A g^{-1}) but also fast kinetics with nearly 93.4% (at 3 mV s^{-1}) capacitive contribution. Through similar strategy, Zha et al. (Zha et al., 2015) prepared capacitive electrode via on-surface synthesis of $COF_{DAAQ\,BTA}$ thin film on 3D graphene. Nevertheless, the cycle stability was not ideal owing to the electrostatic repulsion accumulation and the loss of active materials during repeating cycles. These meaningful explorations provide rich instructions for improving material utilization efficiency and optimizing electrode preparation process.

3.3.3. Flexible supercapacitors

Flexible supercapacitors are in great demand with the rapid development of wearable and flexible electronic equipment, which requires light-weight electrodes bearing high surface area, precisely integrated redox functional groups, and flexible free-standing capability with high mechanical strength. This section

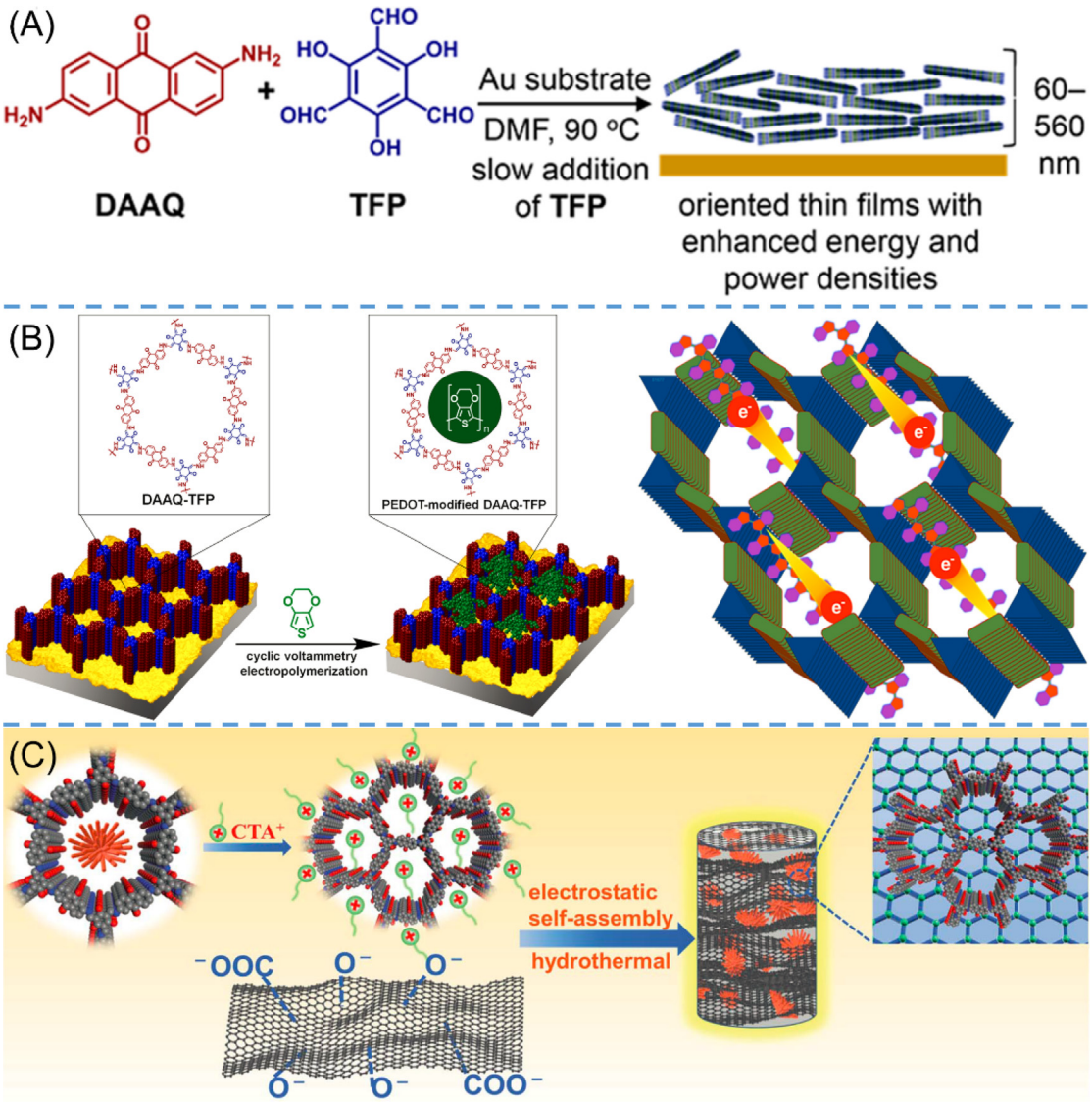

Fig. 10. (A) Schematic illustration of the solvothermal growth of oriented DAAQ-TFP COF thin film on Au electrode (DeBlase et al., 2015). (**B**) Schematic representation of the preparation of PEDOT-modified DAAQ-TFP film (left, Mulzer et al., 2016) and the electron highways of PEDOT@AQ-COF (right, Wu et al., 2019)(Mulzer et al., 2016). (**C**) Schematic diagram of fabrication for DAAQ-COFs/GA composite (An et al., 2021).

will discuss how to achieve these goals through appropriate material design and electrode preparation optimizations.

From the viewpoint of active materials, instead of β-ketoenamine-based DAAQ-TFP, Halder et al. (Halder et al., 2018) prepared an imine-based TpOMe-DAQ COF through convenient mechano-chemical grinding followed by drop casting (Fig. 11A). Due to the rich interlayer C—H···N H-bonding, TpOMe-DAQ not only showed superior chemical stability under harsh conditions but also could generate free-standing thin sheets (~200 μm) in centimeter scale uniformly and continuously. The COF thin film was directly utilized as capacitive electrode with H_2SO_4 (2 M or 3 M) as an electrolyte, and the device exhibited extraordinarily high areal capacitance of 1600 mF cm^{-2} and excellent cycle stability (Table 3 entry 15), which are both important indicators for flexible supercapacitor. Focusing on the intermolecular interactions, the same group further designed and synthesized free-standing flexible thin films by virtue of solid-state molecular baking strategy (Khayum et al., 2018). π-electron-rich 2,6-diaminoanthracene was incorporated to copolymerize with redox-active and electron-withdrawing anthraquinone to enhance the mechanical strength of resulting thin sheet via the optimization of noncovalent interactions between crystallites (Fig. 11B). Among different compositions, Dq_1Da_1Tp COF was found to show balance properties between good mechanical strength and specific capacitance (111F/g). Both TpOMe-DAQ and Dq_1Da_1Tp were assembled into symmetric solid-state supercapacitors. However, the performances of corresponding devices were not very good with low energy density or low power density. Predictably, the low conductivity of COFs might be the main reason.

In order to improve the electrical conductivity of COF thin films, a variety of carbon nanomaterials, which bear excellent electrical conductivity, have been attempted to hybrid with COF. Carbon nanofibers (CNF), which have high aspect ratio and are easy to interpenetrate across each other so as to form flexible films, were included into COF precursor matrixes through in situ solid-state mechanomixing technique (Fig. 12A) by Mohammed (Mohammed et al., 2019). In spite of the weak intermolecular π···π interaction between CNF and COFs, the resulting COF-CNF hybrids yet behaved good electrical conductivity (DqTp-CNF: 2.5×10^{-4} S cm^{-1} and DqDaTp-CNF: 5.2×10^{-5} S cm^{-1}) and high

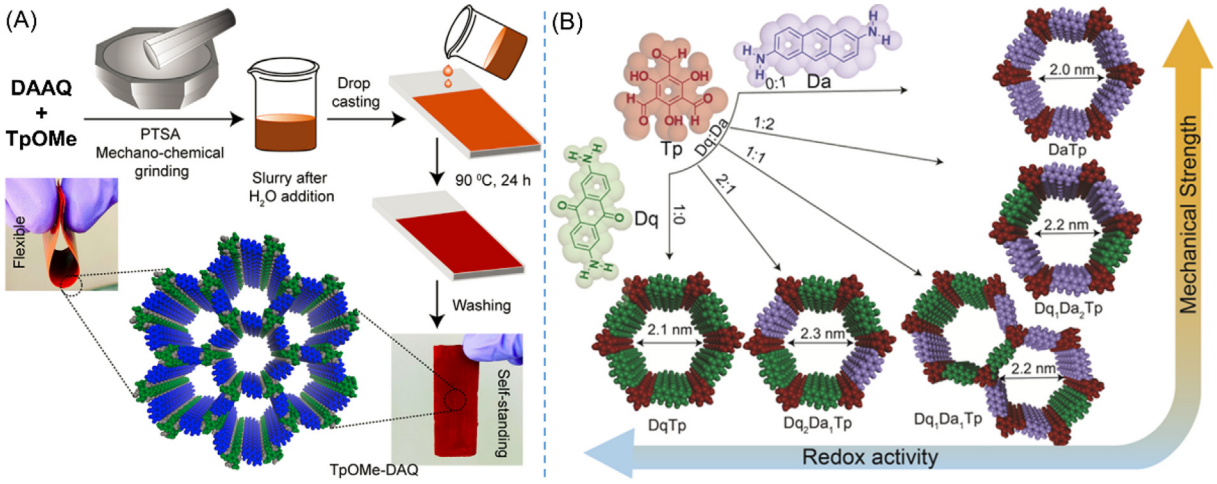

Fig. 11. (**A**) Schematic diagram of the synthesis procedure of the TpOMe-DAQ thin film and its self-standing feature (Halder et al., 2018). (**B**) Schematic illustrations of the modulation of redox activity and mechanical strength of convergent COFs bearing different ratios of monomers (Khayum et al., 2018).

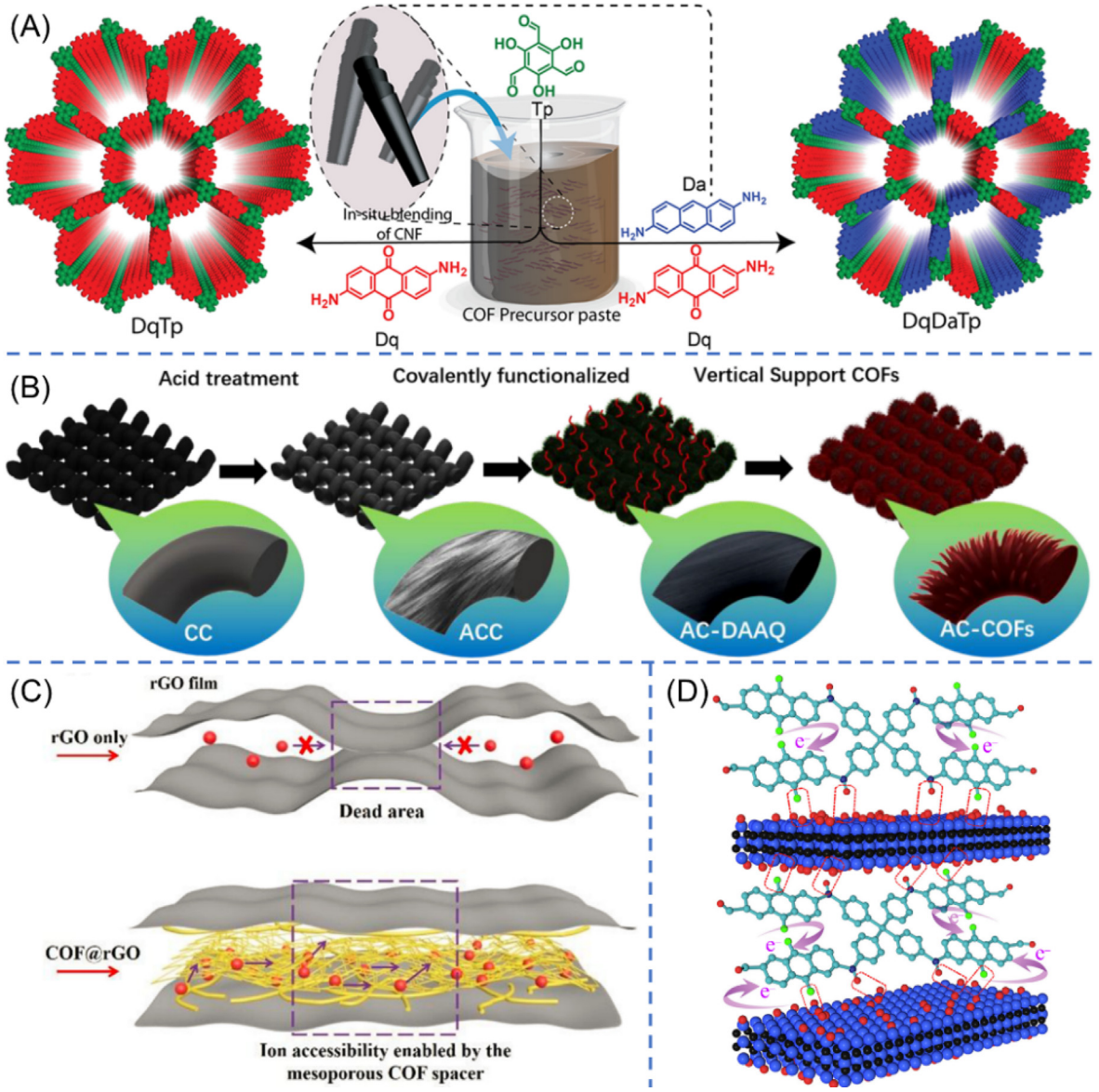

Fig. 12. (**A**) Schematic diagram of the preparation of DqTp-CNF and DqDaTp-CNF COFs. The COFs stack on the graphene layers of the CNF via π···π interactions (Mohammed et al., 2019). (**B**) Schematic illustration of the preparation of functionalized AC-COFs (He et al., 2022). (**C**) Schematic representation of the mechanism of COF@rGO for improving ion transportation (Yao et al., 2022). (**D**) Schematic depiction of the H-bonding interactions between PDT chain and $Ti_3C_2T_x$ sheets and the facilitated electron transfer in the hybrid materials (Wu et al., 2019).

performances for electrochemical energy storage (DqTp-CNF: 464 mF cm^{-2} and DqDaTp-CNF: 364 mF cm^{-2} at 0.25 mA cm^{-2}). In particular, the electrical conductivity of hybrid showed more than 10^9-fold increment in comparison to the pristine COFs. With better mechanical robustness, DqDaTp-CNF hybrid material (with 20% CNF) was assembled into a flexible supercapacitor device that presented a high areal capacitance of 167 mF cm^{-2} (at 0.5 mA cm^{-2}), and the energy density as well as the power density were also improved (Table 3 entry 17). By the way, carboxylated carbon nanotubes (c-CNTs), bearing high aspect ratio but hollow structure, could also be used to fabricate flexible supercapacitors (c-CNT@COF-3 in Table 3 entry 18) (Kong et al., 2021).

Although improving in conductivity, another problem arises because of the weak interactions between COF and CNF would lead to performance degradation (76% after 4500 cycles for DqDaTp-CNF). To address this issue, He et al. (He et al., 2022) integrated redox-active COFs onto the surface of carbon fibers (AC-COFs in Fig. 12B) via strong covalent bridging method. As shown in the figure, partial DAAQ monomer was grafted onto carboxylated carbon fibers to serve as nucleation sites to manipulate the morphology and the growth orientation of DAAQ-TFP COF, and then the polymerization was conducted in situ on the surface of AC-DAAQ. The resulting AC-COFs exhibited a structure of vertical tentacle-like arrays, which noy only could be benefit to capture more electrolyte ions but also could prevent COF from aggregating/collapsing. Accordingly, the capacitance, the cycle stability, the energy density, and the power density were all greatly enhanced (Table 3 entry 19). Xu et al. (Xu et al., 2020) found another approach to enhance the interactions by introducing hydroxyl-ended hyperbranched polymer (OHP) in which the abundant hydroxyl groups intensively interacted with active material and conductive material. Nevertheless, the charge–discharge stability decreased to 80% upon long-term cycles (COF@OHP in Table 3 entry 20), which was probably due to the existence of a large number of weak fatty ester bonds in the OHP.

Graphene bearing sheet structure represents another attractive conductive carbon material on account of its synthetic diversity, good conductivity, and high specific surface area. Moreover, π···π interactions between graphene sheets and other guests allow them to form flexible and highly conductive films. Considering the diverse advantages of graphene, Yao et al. (Yao et al., 2022) introduced reduced graphene oxide (rGO) sheets into DAAQ-TFP COF via in situ synthesis method. On one hand, the incorporation of rGO is helpful to improve the conductivity of materials. On the other hand, by virtue of the intermolecular π − π interaction between rGO nanosheets and COF layers, the few-layer COF plays a role of nanospacer to prevent the rGO nanosheets from accumulating, leading to effective electrolyte ion transport (Fig. 12C). Through the synergistic effect as mentioned above, the prepared flexible COF@rGO microsupercapacitor exhibited superior electrochemical energy storage (Table 3 entry 21). To prevent the re-stacking of graphene sheets, Jang et al. (Jang et al., 2022) modified the graphene via acid reflux activation. The porosity, surface area, and flake size of graphene could be well modulated by varying the acid treatment times. Therefore, the performances of corresponding devices were further enhanced based on anthraquinonylamine-based CMP and activated graphene (CMAP@A4G in Table 3 entry 22).

In addition to carbon materials, Wu et al. (Wu et al., 2019) firstly introduced nonmetallic inorganic material to gain highly flexible supercapacitor electrode. In their study, anthraquinone-based PDT CMP was in situ composited with layered MXene ($Ti_3C_2T_x$) that has high metallic conductivity. The PDT polymer and the MXene could form strong hydrogen bonds between the N—H or C═O bonds of PDT and the oxygen, fluorine or hydroxyl terminal groups on the $Ti_3C_2T_x$ sheets surfaces (Fig. 12D). The H-bonding interactions not only supply precise pathways for charge transportation but also effectively prevent the device from swelling and shrinking upon long-term charge–discharge cycles, giving rise to high capacitance and excellent cycling stability. Remarkably, the film supercapacitor showed outstanding flexibility and cycle stability (97% capacitance retention) through 0 − 90° static bending test for 10,000 cycles. Considering the diversity of anthraquinone-based POPs and nonmetallic sheet materials, this work provides a novel pathway to fabricate flexible supercapacitors with excellent electrochemical performances and superior mechanical toughness.

4. Conclusions and perspectives

Anthraquinone-based POPs have been constructed from many types of reactions such as condensation reactions, coupling reactions, nucleophilic aromatic substitution reactions, and Diels − Alder reaction. Rich adjustable molecular structures together with the merits of high surface area, rigid molecular skeleton, and excellent redox kinetics make them excellent materials for electrochemical energy conversion and storage. In regard to electrocatalysis, anthraquinone-based POPs are mostly used as support materials or precursors, and they play important roles in multiple processes including CO_2RR, ORR, and HER. When directly served as active materials, anthraquinone-based POPs are excellent candidate materials for electrochemical energy storage that contains various rechargeable batteries and supercapacitors. Bottom-up synthesis strategy and post-modification strategy are both utilized to manipulate the aggregation state and the morphology of active materials so as to increase the specific surface areas and improve the accessibility of active sites. There are many practical methods that have achieved good results, such as selecting twisted structure monomers, miniemulsion-solvothermal preparation method, in situ polymerization approach, and exfoliation strategy. To resolve the poor conductivity problem of POPs, various types of superior conductive materials are introduced to form hybrid materials, such as carbon nanotube, graphene, conductive polymer (e.g., PEDOT), and Mxene. Moreover, a number of methods have been exploited to enhance the interactions between these conductive materials and active materials, such as solid-state polymerization approach, preparing hybrid aerogel, and pre-activation treatment. Some polymers have achieved extraordinary success. Taking DAAQ-TFP COF for example, according to the multiple material designs and electrode engineering strategies proposed above, it has been simultaneously applied to a variety of electrochemical processes such as electrocatalysis, rechargeable batteries (e.g., LIB, SIB, PIB, and ZAB), and supercapacitors. These valuable explorations will provide meaningful guidance for material designs and electrode preparation engineering in the future.

Designing and fabricating novel organic materials and electrodes with superior electrochemical performances, meanwhile, with low cost and high availability, still remains a great challenge. The resolution of certain inherent issues, such as enhancing conductivity, chemical stability, and power density, necessitates innovative breakthroughs. Additionally, the intricate synthesis process poses a significant challenge for the practical implementation of anthraquinone-based POPs. There are several attractive aspects that are worthy of constant exploration and pursuit: (1) the increase of theoretical capacity. In addition to polymerization with other electroactive building blocks, further derivation of anthraquinone is also a good choice. 2,3,6,7-Anthraquinonetetracar boxylic dianhydride, which has a higher theoretical capacity of 462 mAh g^{-1}, might be an ideal building block to construct anthraquinone diimide-based POPs. Moreover, its molecular size is smaller than those of commonly used conjugate anhydride (e.g., 1,4,5,8-

naphthalenetetracarboxylic dianhydride and 3,4,9,10-perylenete tracarboxylic dianhydride), meaning it is easier to prepare porous organic polymers with more regular structure. (2) Mechanism study. Electrochemical energy conversion and storage involves various electron transfer and mass transport processes. Gaining profound insight into each specific process and its influencing factors would be of significant importance for designing more efficient devices. (3) Electrode engineering. Developing more convenient electrode preparation technology, improving the dispersion and load capacity of POPs on electrode, exploring new flexible electrode preparation methods, and developing commercially viable electrode preparation technology for large scale production are all worthy of the sweat and effort of chemists, physicists, and materials scientists.

Declaration of Competing Interest

The authors declare that they have no known competing financial interests or personal relationships that could have appeared to influence the work reported in this paper.

Acknowledgement

This document is the results of the research project funded by the National Natural Science Foundation of China (No. 22001026), the Chongqing Science and Technology Commission (CSTC) (No. cstc2020jcyj-msxmX0821), the Chongqing Municipal Education Commission (No. KJQN201900845, No. KJQN202100831), and Scientific Research Foundation for Advanced Talents, Chongqing Technology and Business University (No. 1956054, No. 2056014).

References

Amin, K., Mao, L., Wei, Z., 2019. Recent progress in polymeric carbonyl-based electrode materials for lithium and sodium ion batteries. Macromol. Rapid Commun. 40, 1800565.
Amin, K., Zhang, J., Zhou, H.-Y., et al., 2020. Surface controlled pseudo-capacitive reactions enabling ultra-fast charging and long-life organic lithium ion batteries. Sustain. Energ. Fuels 4, 4179–4185.
An, N., Guo, Z., Xin, J., et al., 2021. Hierarchical porous covalent organic framework/graphene aerogel electrode for high-performance supercapacitors. J. Mater. Chem. A 9, 16824–16833.
Bhambri, H., Khullar, S., Sakshi, et al, 2022. Nitrogen-rich covalent organic frameworks: a promising class of sensory materials. Mater. Adv. 3, 19−124.
Buyukcakir, O., Ryu, J., Joo, S.H., et al., 2020. Lithium accommodation in a redox-active covalent triazine framework for high areal capacity and fast-charging lithium-ion batteries. Adv. Funct. Mater. 30, 2003761.
Byun, Y., Coskun, A., 2018. Epoxy-functionalized porous organic polymers via the Diels-Alder cycloaddition reaction for atmospheric water capture. Angew. Chem. Int. Ed. 57, 3173–3177.
Cao, Y., Sun, W., Guo, C., et al., 2022. Rational construction of yolk–shell bimetal-modified quinonyl-rich covalent organic polymers with ultralong lithium-storage mechanism. ACS Nano 16, 9830–9842.
Cao, Z., Wang, M., Gao, H., et al., 2022. Porous organic polymers via Diels-Alder reaction for the removal of Cr(VI) from aqueous solutions. ACS Macro Lett. 11, 447–451.
Choi, W., Harada, D., Oyaizu, K., et al., 2011. Aqueous electrochemistry of poly (vinylanthraquinone) for anode-active materials in high-density and rechargeable polymer/air batteries. J. Am. Chem. Soc. 133, 19839–19843.
Cui, H., Hu, P., Zhang, Y., et al., 2020. Research progress of high-performance organic material pyrene-4,5,9,10-tetraone in secondary batteries. ChemElectroChem 8, 352–359.
Das, S., Heasman, P., Ben, T., et al., 2017. Porous organic materials: strategic design and structure-function correlation. Chem. Rev. 117, 1515–1563.
DeBlase, C.R., Silberstein, K.E., Truong, T.T., et al., 2013. beta-Ketoenamine-linked covalent organic frameworks capable of pseudocapacitive energy storage. J. Am. Chem. Soc. 135, 16821–16824.
DeBlase, C.R., Hernandez-Burgos, K., Silberstein, K.E., et al., 2015. Rapid and efficient redox processes within 2D covalent organic framework thin films. ACS Nano 9, 3178–3183.
Deng, Q., Luo, Z., Yang, R., et al., 2020. Toward organic carbonyl-contained small molecules in rechargeable batteries: a review of current modified strategies. ACS Sustain. Chem. Eng. 8, 15445–15465.
Deng, Z., Zhao, H., Cao, X., et al., 2022. Enhancing built-in electric field via molecular dipole control in conjugated microporous polymers for boosting charge separation. ACS Appl. Mater. Interfaces 14, 35745–35754.
Duan, J., Wang, W., Zou, D., et al., 2022. Construction of a few-layered COF@CNT composite as an ultrahigh rate cathode for low-cost K-ion batteries. ACS Appl. Mater. Interfaces 14, 31234–31244.
Ega, S.P., Srinivasan, P., 2022. Quinone materials for supercapacitor: Current status, approaches, and future directions. J. Energy Storage 47, 103700.
Evans, A.M., Strauss, M.J., Corcos, A.R., et al., 2022. Two-dimensional polymers and polymerizations. Chem. Rev. 122, 442–564.
Fontmorin, J.-M., Guiheneuf, S., Godet-Bar, T., et al., 2022. How anthraquinones can enable aqueous organic redox flow batteries to meet the needs of industrialization. Curr. Opin. Colloid Interface Sci. 61, 101624.
Geng, K., Arumugam, V., Xu, H., et al., 2020. Covalent organic frameworks: Polymer chemistry and functional design. Prog. Polym. Sci. 108, 101288.
Geng, K., He, T., Liu, R., et al., 2020. Covalent organic frameworks: design, synthesis, and functions. Chem. Rev. 120, 8814–8933.
Geng, Q., Wang, H., Wang, J., et al., 2022. Boosting the capacity of aqueous Li-ion capacitors via pinpoint surgery in nanocoral-like covalent organic frameworks. Small Methods 8, 2200314.
Grieco, R., Molina, A., Sanchez, J. S., et al, 2022. A significantly improved polymer||Ni (OH)2 alkaline rechargeable battery using anthraquinone-based conjugated microporous polymer anode. Mater. Today Energy 27, 101014.
Gu, S., Wu, S., Cao, L., et al., 2019. Tunable redox chemistry and stability of radical intermediates in 2D covalent organic frameworks for high performance sodium ion batteries. J. Am. Chem. Soc. 141, 9623–9628.
Guan, X., Li, H., Ma, Y., et al., 2019. Chemically stable polyarylether-based covalent organic frameworks. Nat. Chem. 11, 587–594.
Guo, C., Liu, M., Gao, G.-K., et al., 2022. Anthraquinone covalent organic framework hollow tubes as binder microadditives in Li-S batteries. Angew. Chem. Int. Ed. 61, e202113315.
Guo, C., Zhou, J., Chen, Y., et al., 2022. Synergistic manipulation of hydrogen evolution and zinc ion flux in metal-covalent organic frameworks for dendrite-free Zn-based aqueous batteries. Angew. Chem. Int. Ed. 61, e202210871.
Halder, A., Ghosh, M., Khayum, M.A., et al., 2018. Interlayer hydrogen-bonded covalent organic frameworks as high-performance supercapacitors. J. Am. Chem. Soc. 140, 10941–10945.
Han, C., Li, H., Shi, R., et al., 2019. Organic quinones towards advanced electrochemical energy storage: recent advances and challenges. J. Mater. Chem. A 7, 23378–23415.
Häupler, B., Wild, A., Schubert, U.S., 2015. Carbonyls: powerful organic materials for secondary batteries. Adv. Energy Mater. 5, 1402034.
He, Y., An, N., Meng, C., et al., 2022. COF-based electrodes with vertically supported tentacle array for ultrahigh stability flexible energy storage. ACS Appl. Mater. Interfaces 14, 57328–57339.
He, Y., An, N., Meng, C., et al., 2022. High-density active site COFs with a flower-like morphology for energy storage applications. J. Mater. Chem. A 10, 11030–11038.
Hu, M.-M., Huang, H., Gao, Q., et al., 2021. Anthraquinone-based covalent organic framework nanosheets with ordered porous structures for highly reversible sodium storage. Energy Fuels 35, 1851–1858.
Jang, M., Cho, Y., Kim, Y., et al., 2022. Redox-active conjugated microporous anthraquinonylamine-based polymer network grafted with activated graphene toward high-performance flexible asymmetric supercapacitor electrodes. Electrochim. Acta 434, 141315.
Kang, H., Liu, H., Li, C., et al., 2018. Polyanthraquinone-triazine−a promising anode material for high-energy lithium-ion batteries. ACS Appl. Mater. Interfaces 10, 37023–37030.
Khayum, M.A., Vijayakumar, V., Karak, S., et al., 2018. Convergent covalent organic framework thin sheets as flexible supercapacitor electrodes. ACS Appl. Mater. Interfaces 10, 28139–28146.
Kim, K.C., 2017. Design strategies for promising organic positive electrodes in lithium-ion batteries: quinones and carbon materials. Ind. Eng. Chem. Res. 56, 12009–12023.
Kim, T., Lee, J., Kim, N., et al., 2022. Redox-active polyimides for energy conversion and storage: from synthesis to application. Chem. Commun. 59, 153–169.
Kong, X., Zhou, S., Strømme, M., et al., 2021. Redox active covalent organic framework-based conductive nanofibers for flexible energy storage device. Carbon 171, 248–256.
Lee, J.M., Cooper, A.I., 2020. Advances in conjugated microporous polymers. Chem. Rev. 120, 2171–2214.
Li, Y., Liu, L., Liu, C., et al., 2019. Rechargeable aqueous polymer-air batteries based on polyanthraquinone anode. Chem 5, 2159–2170.
Li, T., Yan, X., Zhang, W.-D., et al., 2020. A 2D donor-acceptor covalent organic framework with charge transfer for supercapacitors. Chem. Commun. 56, 14187–14190.
Liao, Y., Wang, H., Zhu, M., et al., 2018. Efficient supercapacitor energy storage using conjugated microporous polymer networks synthesized from Buchwald-Hartwig coupling. Adv. Mater. 30, 1705710.
Liu, M., Guo, L., Jin, S., et al., 2019. Covalent triazine frameworks: synthesis and applications. J. Mater. Chem. A 7, 5153–5172.
Liu, M., Wang, Y.-R., Ding, H.-M., et al., 2021. Self-assembly of anthraquinone covalent organic frameworks as 1D superstructures for highly efficient CO_2 electroreduction to CH_4. Sci. Bull. 66, 1659–1668.

Lu, Y., Cai, Y., Zhang, Q., et al., 2022. Insights into redox processes and correlated performance of organic carbonyl electrode materials in rechargeable batteries. Adv. Mater. 34, 2104150.
Luo, L.-W., Zhang, C., Xiong, P., et al., 2021. A redox-active conjugated microporous polymer cathode for high-performance lithium/potassium-organic batteries. Sci. China Chem. 64, 72–81.
Luo, L.-W., Ma, W., Dong, P., et al., 2022. Synthetic control of electronic property and porosity in anthraquinone-based conjugated polymer cathodes for high-rate and long-cycle-life Na-organic batteries. ACS Nano 16, 14590–14599.
Luo, S., Zeng, Z., Wang, H., et al., 2021. Recent progress in conjugated microporous polymers for clean energy: Synthesis, modification, computer simulations, and applications. Prog. Polym. Sci. 115, 101374.
Mahmood, J., Anjum, M.A.R., Baek, J.-B., 2019. Fused aromatic network structures as a platform for efficient electrocatalysis. Adv. Mater. 31, 1805062.
Mohamed, M.G., Sharma, S.U., Yang, C.-H., et al., 2021. Anthraquinone-enriched conjugated microporous polymers as organic cathode materials for high-performance lithium-ion batteries. ACS Appl. Energy Mater. 4, 14628–14639.
Mohammed, A.K., Vijayakumar, V., Halder, A., et al., 2019. Weak intermolecular interactions in covalent organic framework-carbon nanofiber based crystalline yet flexible devices. ACS Appl. Mater. Interfaces 11, 30828–30837.
Molina, A., Patil, N., Ventosa, E., et al., 2019. New Anthraquinone-based conjugated microporous polymer cathode with ultrahigh specific surface area for high-performance lithium-ion batteries. Adv. Funct. Mater. 30, 1908074.
Molina, A., Patil, N., Ventosa, E., et al., 2020. Electrode engineering of redox-active conjugated microporous polymers for ultra-high areal capacity organic batteries. ACS Energy Lett. 5, 2945–2953.
Mulzer, C.R., Shen, L., Bisbey, R.P., et al., 2016. Superior charge storage and power density of a conducting polymer-modified covalent organic framework. ACS Cent. Sci. 2, 667–673.
Oka, K., Murao, S., Kataoka, M., et al., 2021. Hydrophilic anthraquinone-substituted polymer: Its environmentally friendly preparation and efficient charge/proton-storage capability for polymer–air secondary batteries. Macromolecules 54, 4854–4859.
Ouyang, Z., Tranca, D., Zhao, Y., et al., 2021. Quinone-enriched conjugated microporous polymer as an organic cathode for Li-ion batteries. ACS Appl. Mater. Interfaces 13, 9064–9073.
Pan, B., Huang, J., Feng, Z., et al., 2016. Polyanthraquinone-based organic cathode for high-performance rechargeable magnesium-ion batteries. Adv. Energy Mater. 6, 1600140.
Peng, H., Yu, Q., Wang, S., et al., 2019. Molecular design strategies for electrochemical behavior of aromatic carbonyl compounds in organic and aqueous electrolytes. Adv. Sci. 6, 1900431.
Ruan, W., Mao, J., Chen, Q., 2021. Redox flow batteries toward more soluble anthraquinone derivatives. Curr. Opin. Electroche. 29, 100748.
Segura, J.L., Mancheño, M.J., Zamora, F., 2016. Covalent organic frameworks based on Schiff-base chemistry: synthesis, properties and potential applications. Chem. Soc. Rev. 45, 5635–5671.
Son, E.J., Kim, J.H., Kim, K., et al., 2016. Quinone and its derivatives for energy harvesting and storage materials. J. Mater. Chem. A 4, 11179–11202.
Song, Z., Qian, Y., Gordin, M.L., et al., 2015. Polyanthraquinone as a reliable organic electrode for stable and fast lithium storage. Angew. Chem. Int. Ed. 54, 13947–13951.
Song, Z., Miao, L., Ruhlmann, L., et al., 2021. Self-assembled carbon Ssuperstructures achieving ultra-stable and fast proton-coupled charge storage kinetics. Adv. Mater. 33, 2104148.
Song, Y., Zhang, D., Hao, L., et al., 2019. Green synthesis of o-hydroxyazobenzene porous organic polymer for efficient adsorption of aromatic compounds. J. Chromatogr. A 1583, 39–47.
Symons, P., 2021. Quinones for redox flow batteries. Curr. Opin. Electroche. 29, 100759.
Tang, M., Li, H., Wang, E., et al., 2018. Carbonyl polymeric electrode materials for metal-ion batteries. Chinese Chem. Lett. 29, 232–244.
Wang, H., Hou, B., Yang, Y., et al., 2018. Cobalt nanocrystals encapsulated in heteroatom-rich porous carbons derived from conjugated microporous polymers for efficient electrocatalytic hydrogen evolution. Small 14, 1803232.
Wang, Y., Li, Y., Wang, Z., et al., 2020. Reticular chemistry in electrochemical carbon dioxide reduction. Sci. China Mater. 63, 1113–1141.
Wang, S., Wang, Q., Shao, P., et al., 2017. Exfoliation of covalent organic frameworks into few-layer redox-active nanosheets as cathode materials for lithium-ion batteries. J. Am. Chem. Soc. 139, 4258–4261.
Wang, X., Wang, G., He, X., 2023. Anthraquinone porous polymers with different linking patterns for high performance zinc-organic battery. J. Colloid Interf. Sci. 629, 434–444.
Wang, H., Yao, C.-J., Nie, H.-J., et al., 2020. Recent progress in carbonyl-based organic polymers as promising electrode materials for lithium-ion batteries (LIBs). J. Mater. Chem. A 8, 11906–11922.
Wang, H.-G., Zhang, X.-B., 2018. Organic carbonyl compounds for sodium-ion batteries: recent progress and future perspectives. Chem Eur J 24, 18235–18245.
Wang, X., Zhou, J., Tang, W., 2021. Poly(dithieno[3,2-b:2',3'-d]pyrrole) twisting redox pendants enabling high current durability in all-organic proton battery. Energy Storage Mater. 36, 1–9.
Wu, X., Huang, B., Lv, R., et al., 2019. Highly flexible and low capacitance loss supercapacitor electrode based on hybridizing decentralized conjugated polymer chains with MXene. Chem. Eng. J. 378, 122246.
Wu, X., Huang, B., Wang, Q., et al., 2019. Thermally chargeable supercapacitor using a conjugated conducting polymer: Insight into the mechanism of charge-discharge cycle. Chem. Eng. J. 373, 493–500.
Wu, Y., Yan, D., Zhang, Z., et al., 2019. Electron highways into nanochannels of covalent organic frameworks for high electrical conductivity and energy storage. ACS Appl. Mater. Interfaces 11, 7661–7665.
Xu, Z., Liu, Y., Wu, Z., et al., 2020. Construction of extensible and flexible supercapacitors from covalent organic framework composite membrane electrode. Chem. Eng. J. 387, 124071.
Xu, S., Luo, Y., Tan, B., 2013. Recent development of hypercrosslinked microporous organic polymers. Macromol. Rapid Commun. 34, 471–484.
Xu, J., Xu, Y., Lai, C., et al., 2021. Challenges and perspectives of covalent organic frameworks for advanced alkali-metal ion batteries. Sci. China Chem. 64, 1267–1282.
Yan, D., Wu, Y., Kitaura, R., et al., 2019. Salt-assisted pyrolysis of covalent organic frameworks to porous heteroatom-doped carbons for supercapacitive energy storage. J. Mater. Chem. A 7, 26829–26837.
Yang, X., Gong, L., Liu, X., et al., 2022. Mesoporous polyimide-linked covalent organic framework with multiple redox-active sites for high-performance cathodic Li storage. Angew. Chem. Int. Ed. 61, e202207043.
Yang, H., Lee, J., Cheong, J.Y., et al., 2021. Molecular engineering of carbonyl organic electrodes for rechargeable metal-ion batteries: fundamentals, recent advances, and challenges. Energ. Environ. Sci. 14, 4228–4267.
Yao, M., Guo, C., Geng, Q., et al., 2022. Construction of anthraquinone-containing covalent organic frameworks/graphene hybrid films for a flexible high-performance microsupercapacitor. Ind. Eng. Chem. Res. 61, 7480–7488.
Yao, B., Zhou, Y., Ye, X., et al., 2017. A star-shaped molecule with low-yying lowest unoccupied molecular orbital nevel, n-type panchromatic flectrochromism, and long-term stability. Org. Lett. 19, 1990–1993.
Yu, Z., Huang, L., Sun, Z., et al., 2022. Designing anthraquinone-based conjugated microporous polymers with dual-ion storage behavior towards high-performance lithium-organic batteries. J. Power Sources 550, 232149.
Yu, F., Zhu, Z., Li, C., et al., 2022. A redox-active perylene-anthraquinone donor-acceptor conjugated microporous polymer with an unusual electron delocalization channel for photocatalytic reduction of uranium (VI) in strongly acidic solution. Appl. Catal. B: Environ. 314, 121467.
Yuan, D., Dou, Y., Wu, Z., et al., 2022. Atomically thin materials for next-generation rechargeable batteries. Chem. Rev. 122, 957–999.
Zha, Z., Xu, L., Wang, Z., et al., 2015. 3D graphene functionalized by covalent organic framework thin film as capacitive electrode in alkaline media. ACS Appl. Mater. Interfaces 7, 17837–17843.
Zhang, Q., Cui, X., Hao, S., et al., 2021. Chain engineering of carbonyl polymers for sustainable lithium-ion batteries. Mater. Today 50, 170–198.
Zhang, Q., Dou, Y., He, Q., et al., 2022. Emerging carbonyl polymers as sustainable electrode materials for lithium-free metal-ion batteries. Energy Environ. Mater. 5, 1037–1059.
Zhang, Y., Huang, Z., Ruan, B., et al., 2020. Design and synthesis of polyimide covalent organic frameworks. Macromol. Rapid Commun. 41, 2000402.
Zhang, S., Xia, W., Yang, Q., et al., 2020. Core-shell motif construction: Highly graphitic nitrogen-doped porous carbon electrocatalysts using MOF-derived carbon@COF heterostructures as sacrificial templates. Chem. Eng. J. 396, 125154.
Zhang, J., Zhang, G., Jin, S., et al., 2020. Graphitic N in nitrogen-Doped carbon promotes hydrogen peroxide synthesis from electrocatalytic oxygen reduction. Carbon 163, 154–161.
Zhao, H., Chen, H., Xu, C., et al., 2021. Charge storage mechanism of an anthraquinone-derived porous covalent organic framework with multiredox sites as anode material for lithium-ion battery. ACS Appl. Energy Mater. 4, 11377–11385.
Zhao, Q., Guo, C., Lu, Y., et al., 2016. Rechargeable lithium batteries with electrodes of small organic carbonyl salts and advanced electrolytes. Ind. Eng. Chem. Res. 55, 5795–5804.
Zhao, Q., Zhu, Z., Chen, J., 2017. Molecular engineering with organic carbonyl electrode materials for advanced stationary and redox flow rechargeable batteries. Adv. Mater. 29, 1607007.
Zhi, Y., Ma, S., Xia, H., et al., 2019. Construction of donor-acceptor type conjugated microporous polymers: A fascinating strategy for the development of efficient heterogeneous photocatalysts in organic synthesis. Appl. Catal. B: Environ. 244, 36–44.
Zhong, L., Fang, Z., Shu, C., et al., 2021. Redox donor-acceptor conjugated microporous polymers as ultralong-lived organic anodes for rechargeable air batteries. Angew. Chem. Int. Ed. 60, 10164–10171.
Zhou, J., Bai, Y., Qiu, Q., et al., 2023. Ex-situ EPR approach to explore the electrochemical behaviour of Arylboron-Linked conjugated microporous polymer cathode. Chem. Eng. J. 452, 139576.
Zhou, M., Li, X., Zhao, H., et al., 2018. Combined effect of nitrogen and oxygen heteroatoms and micropores of porous carbon frameworks from Schiff-base networks on their high supercapacitance. J. Mater. Chem. A 6, 1621–1629.
Zhu, L., Ding, G., Xie, L., et al., 2019. Conjugated carbonyl compounds as high-performance cathode materials for rechargeable batteries. Chem. Mater. 31, 8582–8612.
Zhu, J., Yuan, S., Wang, J., et al., 2020. Microporous organic polymer-based membranes for ultrafast molecular separations. Prog. Polym. Sci. 110, 101308.